

12-2021

## Contributions to the Heat Capacity of Neutron Stars

Pedro Paulo Barboza Sanson  
*The University of Texas Rio Grande Valley*

Follow this and additional works at: <https://scholarworks.utrgv.edu/etd>



Part of the [Physics Commons](#)

---

### Recommended Citation

Barboza Sanson, Pedro Paulo, "Contributions to the Heat Capacity of Neutron Stars" (2021). *Theses and Dissertations*. 963.

<https://scholarworks.utrgv.edu/etd/963>

This Thesis is brought to you for free and open access by ScholarWorks @ UTRGV. It has been accepted for inclusion in Theses and Dissertations by an authorized administrator of ScholarWorks @ UTRGV. For more information, please contact [justin.white@utrgv.edu](mailto:justin.white@utrgv.edu), [william.flores01@utrgv.edu](mailto:william.flores01@utrgv.edu).

CONTRIBUTIONS TO THE HEAT CAPACITY OF NEUTRON STARS

A Thesis

by

PEDRO PAULO BARBOZA SANSON

Submitted in Partial Fulfillment of the

Requirements for the Degree of

MASTER OF SCIENCE

Major Subject: Physics

The University of Texas Rio Grande Valley

December 2021



CONTRIBUTIONS TO THE HEAT CAPACITY OF NEUTRON STARS

A Thesis  
by  
PEDRO PAULO BARBOZA SANSON

COMMITTEE MEMBERS

Dr. Efrain J. Ferrer  
Chair of Committee

Dr. Vivian Incera  
Committee Member

Dr. Mario Díaz  
Committee Member

December 2021



Copyright 2021 Pedro Paulo Barboza Sanson

All Rights Reserved



## ABSTRACT

Barboza Sanson, Pedro Paulo, Contributions to the heat capacity of Neutron Stars. Master of Science (MS), December, 2021, 50 pp., 2 figures, references, 86 titles.

In this thesis, we review the contribution to the heat capacity of different matter phases that can appear inside a Neutron Star's core, paying special attention to the magnetic dual chiral density wave (MDCDW) phase, which is characterized by an inhomogeneous chiral condensate in the presence of a magnetic field and that is expected to be favored at intermediate densities and low temperatures. Furthermore, we compare our results of the heat capacity for different phases with the observational lower limit of the core heat capacity established from observations of transiently accreting neutron stars which give us crucial information whether certain phases are feasible to appear in the core or not. In particular, we show that the heat capacity of the MDCDW quark-matter phase is well above that lower limit and hence cannot be ruled out.





## DEDICATION

Dedicated to my family, friends and my supervisor Dr. Efrain J. Ferrer. Finally, a special thanks to Gi, without her the difficulties that appeared during the pandemic would have been impossible to withstand.



## ACKNOWLEDGMENTS

This work was possible thanks to NSF Grants PHY-2005331 and PHY-2013222.



## TABLE OF CONTENTS

	Page
ABSTRACT .....	iii
DEDICATION .....	iv
ACKNOWLEDGMENTS .....	v
TABLE OF CONTENTS .....	vi
LIST OF FIGURES .....	viii
CHAPTER I. INTRODUCTION .....	1
1.1 Possible inner structures for neutron star .....	3
1.1.1 Hadronic Star Composition .....	4
1.1.2 Hybrid Star Composition .....	4
1.1.3 Strange Star Composition .....	5
1.2 Neutron Star Cooling .....	5
1.3 How the inner phase of a NS affects its heat capacity .....	6
CHAPTER II. STATISTICAL MECHANICS GENERALITIES .....	9
2.1 The ideal gas in the grand canonical ensemble .....	10
2.2 Neutrality condition for an electron-proton system .....	13
CHAPTER III. THE HEAT CAPACITY OF MAGNETIZED NEUTRON STARS .....	16
3.1 Heat Capacity of Neutron Stars at Low Density .....	16
3.1.1 Heat Capacity of relativistic electrons at low temperature .....	17
3.1.2 Heat Capacity of a Nonrelativistic Superfluid of Neutrons .....	20
3.1.3 Heat Capacity of Superfluid Phonons .....	22
3.2 Heat Capacity of Neutron Stars at High Density .....	23
3.2.1 Heat Capacity of quark matter in the CFL phase .....	23
3.2.2 Heat Capacity of Goldstone modes in the CFL phase .....	25
3.2.3 Heat Capacity of quark matter in the MCFL phase .....	26
3.2.4 Heat Capacity of Goldstone modes in the MCFL phase .....	28

3.3	Heat Capacity of Neutron Stars at Intermediate Density . . . . .	30
3.3.1	Heat Capacity of quark matter in the MDCDW phase . . . . .	31
3.4	Heat Capacity Estimates for Different Neutron Star Compositions . . . . .	34
3.4.1	Nuclear Matter Phase . . . . .	34
3.4.2	Quark Phase . . . . .	38
	CHAPTER IV. CONCLUSION . . . . .	41
	BIBLIOGRAPHY . . . . .	44
	BIOGRAPHICAL SKETCH . . . . .	50

## LIST OF FIGURES

	Page
Figure 1.1: Typical structure of Neutron Star. . . . .	5
Figure 2.1: Dependence of $\mu_e/m_e$ on $\mu/m_e$ . We can observe that $\mu > \mu_e > m_e$ . . . . .	15





## CHAPTER I

### INTRODUCTION

Since the dawn of humanity, stars have been a distinct point of interest and fascination to those who look up to the sky. As we tried to understand the universe around us, an entire field was naturally developed to comprehend the celestial bodies that have been always above us, i.e. astronomy. Stars are the most widely recognizable and most fascinating astronomical objects. The majority of stars are between 1 billion and 10 billion years old, almost as old as the Universe itself and their life cycles are determined by their masses which range from  $0.08M_{\odot}$  to approximately  $300M_{\odot}$ . For the stars with lowest masses, their cores aren't hot enough to stably ignite hydrogen (H), but for most stars they will simply convert H into helium (He) by nuclear fusion and the "chain" of fusion is determined by the mass of the star, i.e., while massive stars can fuse atoms up to iron, low mass stars can convert He into carbon (C) but won't fuse C into heavier elements. Meanwhile, their lifetime will be determined by the supply of H inside the core, once this supply is over, they will no longer generate heat. Therefore, the core becomes increasingly unstable and contracts. At the same time, the outer shell of the star will expand and as it does so, it will cool and become red, transforming the star into a red giant.

For stars with masses  $M > 8M_{\odot}$ , which will fuse helium, oxygen, nitrogen, carbon, and all other elements with higher atomic numbers up to iron. Once the core is formed solely by iron, the star begins its final phase. Fusing iron requires an input of energy since iron is the most stable element. Thus, once it is reached an iron core the fusion is exhausted and without the pressure associated with the outgoing radiation coming from the nuclear fusion reaction, the star starts its grav-

itational collapse. Hence, as temperature rises the repulsive force between nuclei is overwhelmed by the push of gravity and iron atoms are crushed together, and the core responds recoiling out, which we can observe as a supernova explosion, the end of a massive star's life. It is important to notice that, since the core of stars can't fuse iron, heavier elements, such as uranium or gold, can only be produced in these astounding events where there's enough energy to create them.

There are two major types of supernovae, type I (SNI) and type II (SNII). SNI are characterized by not presenting H lines and also a deep absorption in  $6150\text{\AA}$ , while type II (SNII) has clear H lines [1]. The aftermath of a supernova event depends on the mass of the progenitor star, and of the mass of its core. If the mass of the star is  $M > 8M_{\odot}$  and its core had a mass between  $M_{\odot} < M_c < 3M_{\odot}$ , most of the stellar matter will be thrown far from the star during the supernova collapse, but the star's iron-filled inner part will remain as a compact object known as the Neutron Star (NS), one of the most singular objects in the observable universe. For even bigger progenitor masses, the supernova collapse can give rise to a black hole.

The first suggestion or rather anticipation that we had about the existence of NS's came from Lev D. Landau who proposed the idea of a star "forming one gigantic nucleus" and by the end of the 60's the first NS was detected [2]. Today, we not only know about their existence, but we also know that their masses range from  $1.4M_{\odot}$  up to  $2.3M_{\odot}$  and they have radius around (10-13)km, which places them among the densest objects in the observable universe, reaching in their cores several times the nuclear density  $\rho_n = 2.4 \times 10^{14} \text{g/cm}^3$  [3].

Another interesting characteristic of a NS is its magnetic field. They have the strongest magnetic fields found in nature, starting from observable values in their surfaces of  $10^8 \text{G}$  in millisecond pulsars, and reaching in their surfaces between  $10^{13}$  and  $10^{15} \text{G}$  for special NSs known as magnetars [4, 5]. The inner magnetic fields at the core of these magnetars can be even stronger due to magnetic field flux conservation in stellar mediums with very large electric conductivity. In fact, it has been estimated that they are of the order of  $10^{18} \text{G}$  for nuclear matter cores [6] and  $10^{19} - 10^{20} \text{G}$  for quark matter ones [7]. The presence of such large magnetic fields can impact several properties

of such objects, motivating many studies on the equations of state (EoS) of magnetized NS's.

The EoS is a thermodynamic equation that relates the energy density with the system pressure and it characterizes the system state described by the thermodynamic quantities and external fields as temperature, chemical potential, magnetic field, etc. So they are absolutely essential in modeling the structure and evolution of NSs because they are essential to derive the Tolman-Oppenheimer-Volkov (TOV) equations [8] from where the relation between the stellar mass and radius is derived. But since the state of matter existing in the NS interior is still undetermined, the precise determination of the EoS that describe the inner state enclosed in a NS is still an open question.

### 1.1 Possible inner structures for neutron star

Depending of the inner densities that a NS can reach, it can have different structures, which can form hadronic stars, hybrid stars and strange stars. As follows, we describe what are the internal characteristics of each of them.

The two first cases of NSs, hadronic and hybrid, have similar structures and they can be roughly divide in three layers, outer crust, inner crust and the core. The matter density in the outer crust is in the interval  $10^6 \text{g/cm}^3 < \rho < \rho_d$  (where  $\rho_d = 4 \cdot 10^{11} \text{g/cm}^3$  is the drift density), which is not high enough to free nucleons from the nucleus, so they are bound and cannot move freely. Therefore, the configuration in the outer crust can be simply described as a Coulomb lattice of heavy nuclei with a relativistic degenerate electron gas. As the density goes up and gets closer to the neutron drip density  $\rho_d$ , the nuclei have become so rich that the neutron states lying in the continuum will be filled and the lattice of neutron-rich nuclei become permeated with free neutrons. Degenerate neutron Fermi sea will be formed through this process. When entering the inner crust, the density region becomes  $\rho_d < \rho < 0.7\rho_s$ , where  $\rho_s = 2.84 \cdot 10^{14} \text{g/cm}^3$  is the nuclear matter drip density. There, as more neutrons are free, they will interact forming Cooper pairs, and because of the relative low temperatures associated with all but newborn NSs, we will have neutron superfluid

present in the inner crust [9, 10]. Finally, once the density surpass  $0.7\rho_s$  we reach the core which constitutes up to 99% of the stellar mass. Depending on the density that is reached there we can have two different compositions that we will consider as follows.

### **1.1.1 Hadronic Star Composition**

In the hadronic case, the core's density lies between  $\rho_s < \rho < 2.8\rho_s$ . By densities about the order of  $\rho_s$  the atomic nuclei are practically touching each other, and beyond that density they will merge into a liquid composed of mainly neutron, some protons and some electrons, which ensures charge neutrality. At this point, protons will form Cooper pairs and since they aren't electrically neutral, they will form a superconducting fluid; while the neutral neutrons will form a superfluid. Here, it is important to point out that due to the presence of superfluidity and superconductivity both the thermal and dynamical evolution of the NSs are impacted [10, 11]. In this case, since the density doesn't surpass  $2.8\rho_s$ , hadronic matter is still stable and will prevail in the core of the star, hence the name Hadronic Star.

### **1.1.2 Hybrid Star Composition**

In order to discuss the hybrid case, we must first point out that quantum chromodynamics predicts that at sufficiently high densities, quarks will be deconfined leading to a degenerate state of quarks [12]. Here, we are considering NSs with core densities much higher than the previous case,  $5 \sim 10\rho_s$ . Those densities are so high that we can expect that the nuclear/hadronic matter will transition into new phases with more exotic particles, as a new quark matter phase, composed by deconfined quarks and a small mixture of electrons to guarantee electric neutrality, or a phase with a hyperon mixture [13, 14]. In this scenario, the star crust composition will be purely hadronic and the core will have new degrees of freedom due to its massive density. The compact object composed by these two phases is what is called a Hybrid Star.

### 1.1.3 Strange Star Composition

The third case is prompted by the Bodmer–Terazawa–Witten hypothesis [15, 16, 17] which is based on the idea that strange matter has a lower energy per baryon than ordinary nuclei even including  ${}_{56}\text{Fe}$ . Thus, under this hypothesis, the true ground state of the hadrons may be strange matter. Now, if this is indeed the case, then ordinary nuclei would decay into strange quark matter, which is simply a composition of up, down and strange quarks. This process is irreversible, since it would be more stable, and once it starts it is expected that the whole star will convert into the quark composition considered above, making it a pure Strange Star [18, 19].

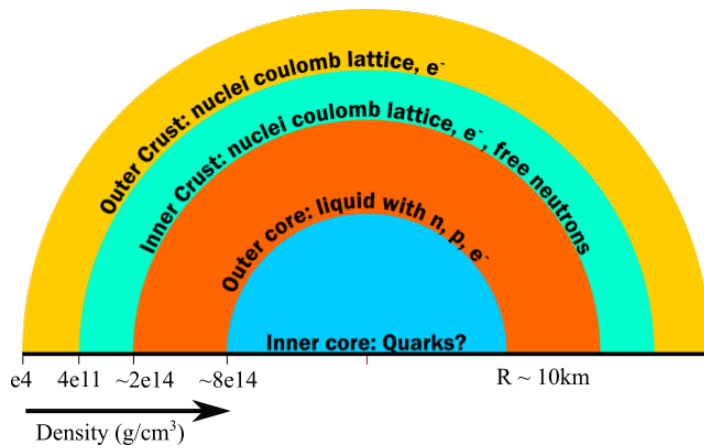


Figure 1.1: Typical structure of Neutron Star.

## 1.2 Neutron Star Cooling

In order to reduce the humongous amount of possible candidates that can serve to define the state of matter in the dense medium existing in the core of NS, we need to find constraints that point us to valid EoS's and, consequently, to predict the most probable inner phases of NS. The combination of mass-radius measurements, for example, already place robust constraints on the EoS, but that alone doesn't seem sufficient to find a unique answer. Recently, LIGO and Virgo made their first observation of a neutron star binary system and this represents a new possibility to measure the EoS of matter in such binaries by looking into deviations in the emitted gravitational

waves because of tidal deformation effects [20].

Another promising approach might be connecting transport properties of different matter phases with the observed behavior of NS cooling. To understand that, we need to acknowledge first that without an active core (i.e., those where no nuclear fusion is happening inside them) the NS internal temperature will inevitably reduce over time and this process can be divided in roughly two stages [21, 22]: (a) When a NS is born its temperature is around  $10^{11}K$ , then its predominant cooling mechanism during at least a thousand years is neutrino emission from the core. (b) Once the temperature decays up to  $10^8K$ , then photon emission from the surface dominates.

Since the interior of a NS is essentially isothermal, we can propose, as a first approximation, that its thermal history takes place through the following energy balance equation [22]

$$-\frac{dE}{dt} = -C_V \frac{dT}{dt} = L_\nu + L_\gamma - H, \quad (1.1)$$

where  $E$  is the internal energy,  $T$  is the inner medium temperature,  $t$  the star's age,  $C_V$  is the heat capacity at constant volume,  $L_\nu$  and  $L_\gamma$  are neutrino and surface photon luminosities respectively, and  $H$  is the heating rate associated with any additional heating source. This equation makes clear that the heat capacity plays a fundamental role in the thermal evolution of the NS. This fact underlines the importance of the results we will report as part of this thesis.

### 1.3 How the inner phase of a NS affects its heat capacity

Depending on the star composition, we will have different matter phases and consequently different thermal properties. To fulfill this analysis, it is useful to start with the extremes cases, that is, to investigate the  $C_V$  for the limit cases of the low and high density regions, because they are easier to work with and give us useful insights. Later, we will consider the more realistic case of a star at intermediate densities.

In the low density case, when  $\rho \sim \rho_s$ , we have a Hadronic Star whose interior contains solely nuclear/hadronic matter in all its internal layers, including the inner core. This means that

we only have to work with a mixture of neutrons, protons and some electrons in order to ensure charge neutrality. These are the only components that will play a role in our calculations of the heat capacity in this case. Nevertheless, we should take into account that despite we are considering the lowest density candidate, such a compact object is dense enough for the occurrence of quantum-relativistic effects that will affect its thermodynamic and transport properties.

In the opposite side, at asymptotically high densities that can be equal or greater than 2-3 times the nuclear matter density, quark deconfinement can take place either inside the core of a Hybrid Star configuration or through out the whole volume of a Strange Star. Now, from QCD studies it is known that at asymptotically high densities the more stable configuration is a color-superconducting phase known as color-flavor-locking (CFL) phase. The idea is that at ultra-high densities the mass of the strange quark becomes negligible small as compared to the baryonic chemical potential leading to the same density of the three flavors, u, d and s quarks. Thus we observe the formation of Cooper pairs between all three colors and all three flavors of quarks coupled with total zero momentum [23].

But in a realistic scenario, NSs don't have asymptotically high densities. As is well known, the CFL phase relies on the assumption that the quarks that pair with equal and opposite momenta can each be arbitrarily close to their common Fermi surface. But, with decreasing density, the combined effect of the strange quark mass, neutrality constraint and beta equilibrium, create a mismatch in the Fermi momenta of different flavors, imposing an extra energy cost on the formation of Cooper pairs. Thus, with decreasing density, the CFL phase eventually becomes gapless and, most importantly, becomes unstable [24, 25]. The instability manifests itself in the form of imaginary Meissner masses for some of the gluons and is known as the chromomagnetic instability. This finding indicates an instability towards spontaneous breaking of translational invariance [26, 27, 28, 29]. In other words, the formation of a spatially inhomogeneous phase takes place.

On the other hand, various QCD effective model studies, as well as QCD calculations in the large- $N_c$  limit [30, 31, 32, 33] indicate that in the region of intermediate densities there exists



some states, which are characterized by inhomogeneous particle-hole condensates, in which the pairs carry a total finite momentum. These studies suggest that the inhomogeneous phases might be unavoidable in the regions of intermediate temperature and density. A systematic and complete investigation to determine the most energetically favored state under different conditions is still open. In this thesis we show the results found for the heat capacity of possible different phases that might be plausible for NS interiors and, in particular, we focus on calculations for the inhomogeneous particle-hole phase, called MDCDW phase, in order to show that such phase satisfies the important observational constraint established for the lower limit of the specific heat of NS, i.e.  $C_V \gtrsim 10^{36} \left(\frac{T}{10^8}\right) \frac{\text{erg}}{\text{K}}$ , showing that, the studied MDCDW phase satisfies this constraint indicating that it can be a reliable candidate to form the interior of NSs.

## CHAPTER II

### STATISTICAL MECHANICS GENERALITIES

The heat capacity  $C$  of a body is defined as the amount of energy needed to increase the body temperature in one degree Kelvin. The specific heat, is then defined as the heat capacity per unit mass,  $C_V = \frac{C}{M}$ . Both, the heat capacity and consequently the specific heat, depend on the state of matter under consideration. For example, the specific heat of water at  $20^\circ\text{C}$  is  $4182 \frac{\text{J}}{\text{K}} \cdot \text{kg}$ ; while that of ice just below  $0^\circ\text{C}$  is only  $2093 \frac{\text{J}}{\text{K}} \cdot \text{kg}$  [34]. Therefore, for most systems, the heat capacity is not constant and will depend on state variables such as temperature, pressure and volume. That is why it is common practice that the heat capacity of gases and liquids is measured at constant pressure or volume.

In light of this, the heat capacity at constant volume is an extensive quantity that can be defined in terms of other thermodynamic quantities as

$$C_V := \left( \frac{dQ}{dT} \right)_V = T \left( \frac{dS}{dT} \right)_V, \quad (2.1)$$

where  $Q$  is the amount of heat transfer,  $S$  the entropy,  $T$  the absolute temperature and  $V$  the volume under consideration.

Since our main goal is to deal with NSs, any model we consider to describe its interior will be formed by a huge amount of particles with many degrees of freedom that are distributed in many different physical states. So, it only makes sense to use a statistical-mechanic description to extract the physical properties of this system.

All the equilibrium properties of a statistical system of particles in contact with a thermal

reservoir can be found by working with the grand canonical potential  $\Omega(T, V, \mu)$ , which depends on the chemical potential  $\mu$  in addition to temperature and volume. The grand canonical potential satisfies the thermodynamic relation

$$\Omega = F(T, V, N) - \mu N, \quad (2.2)$$

where  $F$  is the system Helmholtz free energy and  $N$  the number of particles. Therefore, the total differential of  $\Omega$  is simply

$$\begin{aligned} d\Omega &= \left(\frac{\partial\Omega}{\partial T}\right) dT + \left(\frac{\partial\Omega}{\partial V}\right) dV + \left(\frac{\partial\Omega}{\partial N}\right) dN \\ &= -SdT - PdV - Nd\mu, \end{aligned} \quad (2.3)$$

with  $P$  denoting the pressure.

Combining equations (2.1) and (2.3) we find

$$C_V = -T \left(\frac{d^2\Omega}{dT^2}\right)_V = -2\beta^2 \left(\frac{d\Omega}{d\beta}\right)_V + \beta^3 \left(\frac{d^2\Omega}{dT^2}\right)_V, \quad (2.4)$$

where  $\beta$  denotes the inverse of the absolute temperature ( $\beta = \frac{1}{T}$ ). Equation (2.4) is a useful relation when the grand canonical potential is known [34, 35].

## 2.1 The ideal gas in the grand canonical ensemble

To understand how the heat capacity can be extracted from the grand canonical potential, we briefly discuss how it is obtained for the ideal mono-atomic gas system with volume  $V$  and in contact with a reservoir at temperature  $T$  and chemical potential  $\mu$ .

The grand canonical potential can be defined as:

$$\Omega = -\frac{1}{\beta} \ln Z, \quad (2.5)$$

where  $Z$  is the grand partition function which is given by

$$Z(T, V, \mu) = \sum_{N=0}^{\infty} \frac{1}{N!} \int \frac{d^{3N}q d^{3N}p}{h^{3N}} e^{-\beta(H(q,p,N) - \mu N)} \quad (2.6)$$

In (2.6),  $H$  denotes the system Hamiltonian and  $N!$  comes from the fact that in systems where the particles are indistinguishable, as in an ideal mono-atomic gas, we need to take out the redundant counting introduced by taking into consideration the identical states that are obtained from their permutations [35].

For the ideal gas under consideration, the Hamiltonian is simply its kinetic energy

$$H(p) = \sum_{i=1}^N \frac{\mathbf{p}_i^2}{2m} \quad (2.7)$$

Therefore the grand canonical partition function is

$$Z(T, V, \mu) = \sum_{N=0}^{\infty} \frac{V^N e^{\beta \mu N}}{N!} \left( \int_{-\infty}^{\infty} \frac{dp}{h} e^{-\beta \frac{p^2}{2m}} \right)^{3N} \quad (2.8)$$

We can combine the equation above with the result below

$$\int_{-\infty}^{\infty} dx e^{-x^2} = \sqrt{\pi} \quad (2.9)$$

And now we can calculate the partition function

$$\begin{aligned}
 Z(T, V, \mu) &= \sum_{N=0}^{\infty} \frac{V^N e^{\beta\mu N}}{N!} \left( \frac{\sqrt{2\pi m T}}{h} \right)^{3N} \\
 &= \sum_{N=0}^{\infty} \frac{1}{N!} \left( e^{\beta\mu} \frac{1}{\lambda_T^3} \right)^N \\
 &= \exp \left( e^{\beta\mu} \frac{V}{\lambda_T^3} \right)
 \end{aligned} \tag{2.10}$$

where  $\lambda_T = \frac{h}{\sqrt{2\pi m T}}$  is the thermal de Broglie wave length. Therefore, the grand canonical potential of the ideal gas is

$$\Omega(T, V, \mu) = -\frac{1}{\beta} e^{\beta\mu} \frac{V}{\lambda_T^3} \tag{2.11}$$

From (2.3) and (2.11) we find that the particle number  $N$  is given by

$$N(T, V, \mu) = - \left( \frac{\partial \Omega}{\partial \mu} \right)_{T, V} = e^{\beta\mu} \frac{V}{\lambda_T^3} \tag{2.12}$$

similarly, we can also find the entropy of this system as

$$S(T, V, \mu) = - \left( \frac{\partial \Omega}{\partial T} \right)_{T, \mu} = N \left( \frac{5}{2} - \frac{\mu}{T} \right) \tag{2.13}$$

We can invert the chemical potential inside the parenthesis using (2.12) to get the Sackur-Tetrode equation

$$S = N \left( \ln \frac{V}{N \lambda_T^3} + \frac{5}{2} \right) \tag{2.14}$$

Finally, we can separate the term that depends on temperature using logarithm properties and if the

number of particles remains constant we find the heat capacity to be

$$\begin{aligned}
C_V = T \left( \frac{\partial S}{\partial T} \right)_{V,\mu} &= NT \left( \frac{\partial \left( \frac{3}{2} \ln T + \ln(\dots) \right)}{\partial T} \right)_{V,\mu} \\
&= \frac{3}{2} N
\end{aligned} \tag{2.15}$$

Which is a well known result that is independent of the temperature and is a good approximation to the behavior of noble gases [35]. Furthermore, if we were to derive the pressure by similar steps that were done to find the heat capacity we would find the famous general gas equation  $PV=nRT$ , first stated by Clapeyron.

In the following chapters we will apply similar methods to investigate the heat capacity of different phases of dense matter that could be forming the interior of NSs.

## 2.2 Neutrality condition for an electron-proton system

In this section we estimate the value of the electric chemical potential  $\mu_e$  for a NS, so to get an idea of how important is this chemical potential with respect to other parameters characterizing this compact system.

It is a well accepted fact that NSs are electrically neutral. Because of the difference in magnitude of the electromagnetic and the gravitational force, the net charge must be extremely small, with  $Z_{net} \sim |Z_p - Z_e| < 10^{-36}A$ , where  $Z_p$  and  $Z_e$  are the proton and electron numbers and  $A$  is the baryon number [36].

Here, we consider densities that are not high enough so that we would observe other charged degrees of freedom different than protons and electrons, such as more massive leptons or hyperons. Therefore, the global charge neutrality condition is

$$Q_{net} = Q_e + Q_p = -eN_e + eN_p = e \left( \partial_{\mu_e} \Omega_e - \partial_{\mu_p} \Omega_p \right) = 0 \tag{2.16}$$

Where the chemical potential is given by  $\mu_p = \mu - \mu_e$ ,  $\mu$  is the baryonic chemical potential,  $\mu_e$  is

the electric chemical potential and  $m_e$  is the electron mass.

The thermodynamic potentials for electrons and protons are given respectively by

$$\Omega_e = -\frac{2}{\beta} \int_{-\infty}^{\infty} \frac{d^3 p}{(2\pi)^3} \ln \left[ (1 + e^{-\beta(\varepsilon_e + \mu_e)})(1 + e^{-\beta(\varepsilon_e - \mu_e)}) \right] \quad (2.17)$$

$$\Omega_p = -\frac{2}{\beta} \int_{-\infty}^{\infty} \frac{d^3 p}{(2\pi)^3} \ln \left[ (1 + e^{-\beta(\varepsilon_p + \mu_p)})(1 + e^{-\beta(\varepsilon_p - \mu_p)}) \right], \quad (2.18)$$

and the particle numbers are simply

$$N_e = -\partial_{\mu_e} \Omega_e = \frac{1}{\pi^2} \int_0^{\infty} p^2 dp \left( \frac{1}{(1 + e^{\beta(\varepsilon_e - \mu_e)})} - \frac{1}{(1 + e^{\beta(\varepsilon_e + \mu_e)})} \right) \quad (2.19)$$

$$N_p = -\partial_{\mu_p} \Omega_p = \frac{1}{\pi^2} \int_0^{\infty} p^2 dp \left( \frac{1}{(1 + e^{\beta(\varepsilon_p - \mu_p)})} - \frac{1}{(1 + e^{\beta(\varepsilon_p + \mu_p)})} \right) \quad (2.20)$$

Now we want to use the neutrality equation in order to find the relationship between  $\mu$ ,  $\mu_e$  and  $m_e$ . Considering that  $\mu_e, \mu_p > 0$  and knowing that the electron and proton dispersion relations are respectively,  $\varepsilon = \sqrt{p^2 + m_e^2}$  and  $\varepsilon_p = \sqrt{p^2 + m_p^2}$ , then in the zero-temperature limit we find

$$N_e = \frac{1}{\pi^2} \int_0^{\infty} p^2 dp \theta(\varepsilon_e - \mu_e) = \frac{1}{\pi^2} \int_0^{\sqrt{\mu_e^2 - m_e^2}} p^2 dp = \frac{1}{3\pi^2} [\mu_e^2 - m_e^2]^{3/2} \quad (2.21)$$

$$N_p = \frac{1}{\pi^2} \int_0^{\infty} p^2 dp \theta(\varepsilon_p - \mu_p) = \frac{1}{\pi^2} \int_0^{\sqrt{\mu_p^2 - m_p^2}} p^2 dp = \frac{1}{3\pi^2} [\mu_p^2 - m_p^2]^{3/2} \quad (2.22)$$

From the neutrality condition (2.16), we have that  $N_e = N_p$ , hence it follows that

$$(\mu_e - \mu)^2 - m_p^2 = \mu_e^2 - m_e^2 \quad (2.23)$$

Introducing the notation,  $x = \mu/m_e$  and  $y = \mu_e/m_e$ ; for  $m_e = 0.5$  MeV and  $m_p = 938.3$  MeV, the

neutrality condition (2.23) can be written as

$$y = \frac{1 - 0.4 \times 10^7}{2x} + \frac{x}{2} \quad (2.24)$$

This function is plotted in Fig. 2.1 for the domain of interest for NSs. Since  $y > 0$ , we have that  $x > 2 \times 10^3$ , and we consider  $\mu$  values corresponding up to 10 times nuclear density.

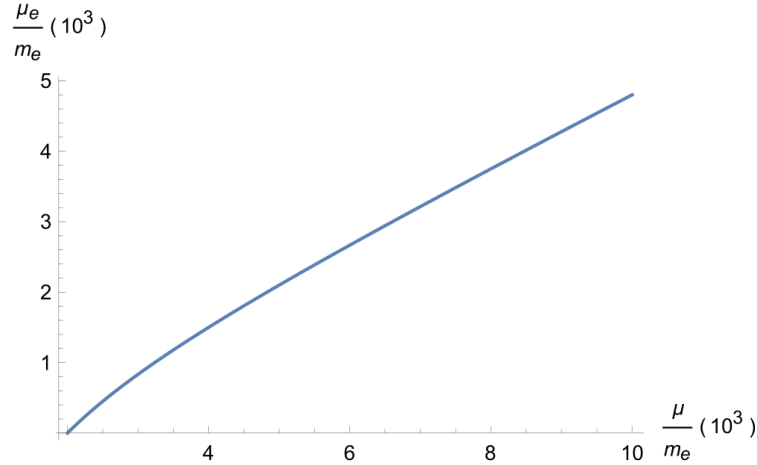


Figure 2.1: Dependence of  $\mu_e/m_e$  on  $\mu/m_e$ . We can observe that  $\mu > \mu_e > m_e$ .

Using the neutrality condition for the NS medium formed by protons and electrons as charged particles, we arrived at Fig. 2.1 where its clear that  $\mu > \mu_e > m_e$ . This justifies neglecting  $m_e$  in Eqs. (3.10) and (3.17) which will be realized in the next Chapter.



## CHAPTER III

### THE HEAT CAPACITY OF MAGNETIZED NEUTRON STARS

In this chapter, we will show how different matter phases that can be realized at different baryon densities can contribute to the heat capacity of NS. In our approach, we are taking into account the effects produced by a magnetic field, since in the stellar medium the presence of a magnetic field is unavoidable.

The chapter is divided in three sections. In Section 3.1, we review calculations of the heat capacity of a relativistic electron gas and of a neutron superfluid at low temperature. Both components are commonly found in NS regions at relatively low baryon densities. There, we will also discuss the effects of the magnetic field on the heat capacity of electrons. In Section 3.2, we calculate the heat capacity of quark matter, first in the CFL phase and then in the MCFL phase, where the magnetic field will be relevant [37]. In Section 3.3, we calculate the heat capacity of the MDCDW phase, which is a phase that can be realized at intermediate densities. In this phase, the magnetic field will play an essential role in guaranteeing the stability of the phase with respect to thermal fluctuations [38]. Finally, in Section 3.4 we estimate the heat capacity values for the parameters (as temperature, density, etc.) characterizing the different NS inner phases.

#### **3.1 Heat Capacity of Neutron Stars at Low Density**

As mentioned in Chapter I, Section 1.3, in the low-density limit NS cores are mainly constituted by nuclear matter. So, we only need to consider as constituents that can ensure electric charge neutrality protons, neutrons and electrons. Moreover, in our calculations we can consider the low-temperature limit,  $T \ll \mu_e, \mu$  where  $\mu_e$  and  $\mu$  are the electric and baryonic chemical po-

tential respectively. Therefore, in order to calculate the heat capacity, we only need to use Eq. (2.4), while paying special attention to quantum-relativistic statistics that are important in the thermodynamic and transport properties inside NSs.

### 3.1.1 Heat Capacity of relativistic electrons at low temperature

For electrons, the NS inner magnetic field is large enough to have a noticeable effect on the heat capacity. Thus, we shall calculate it ignoring the presence of the magnetic field first and then we will compare the result with the one we find when considering the presence of a magnetic field.

#### A. Electrons at $B = 0$

When using formula (2.4), we only need to consider the statistical part of the thermodynamic potential. By performing the Matsubara frequency sum [39, 40], we can obtain the thermodynamic potential in the one-loop approximation at finite temperature and density given by

$$\Omega_\beta^e = -\frac{2}{\beta} \int_{-\infty}^{\infty} \frac{d^3 p}{(2\pi)^3} \left[ \ln(1 + e^{-\beta(\varepsilon_e + \mu_e)}) + \ln(1 + e^{-\beta(\varepsilon_e - \mu_e)}) \right], \quad (3.1)$$

where the energy spectrum is  $\varepsilon_e = \sqrt{p^2 + m_e^2}$  and the factor 2 comes from the spin degeneracy.

Substituting Eq. (3.1) into (2.4), we obtain

$$C_V^e = \frac{1}{16\pi^3 T^2} \int_{-\infty}^{\infty} d^3 p \left[ (\varepsilon_e + \mu_e)^2 \operatorname{sech}^2 \left( \frac{\varepsilon_e + \mu_e}{2T} \right) + (\varepsilon_e - \mu_e)^2 \operatorname{sech}^2 \left( \frac{\varepsilon_e - \mu_e}{2T} \right) \right] \quad (3.2)$$

Assuming that  $\mu_e > 0$ , we can discard, in the low-temperature limit, the positron's contribution in (3.2) such that

$$C_V^e \simeq \frac{1}{4\pi^2 T^2} \int_0^{\infty} dp p^2 (\varepsilon_e - \mu_e)^2 \operatorname{sech}^2 \left( \frac{\varepsilon_e - \mu_e}{2T} \right) \quad (3.3)$$

Now, using the dispersion relation, we can make a variable change to integrate in energy

$$C_V^e \simeq \int_{m_e}^{\infty} d\varepsilon_e g(\varepsilon) \left( \frac{\varepsilon_e - \mu_e}{2T} \right)^2 \operatorname{sech}^2 \left( \frac{\varepsilon_e - \mu_e}{2T} \right) \quad (3.4)$$

where we introduced the density of state per unit volume function

$$g(\varepsilon_e) = \frac{\varepsilon_e \sqrt{\varepsilon_e^2 - m_e^2}}{\pi^2} \quad (3.5)$$

Taking into account the form of the Fermi-Dirac distribution, we have that at low temperatures ( $k_B T < \varepsilon_F$ ), the integral (3.4) only changes significantly in the vicinity of the Fermi energy  $\varepsilon_F$ . Therefore, we can approximate the density of states  $g(\varepsilon)$  by  $g(\varepsilon_F)$  in order to write

$$C_V^e \simeq g(\varepsilon_F) T \int_{\frac{m_e - \varepsilon_F}{T}}^{\infty} \left( \frac{x}{2} \right)^2 \operatorname{sech}^2 \left( \frac{x}{2} \right) dx \quad (3.6)$$

Where the variable change,  $x = \frac{\varepsilon_e - \varepsilon_F}{T}$ , was performed. For  $m_e < \mu_e$ , which is in agreement with the electric neutrality result (see Section 2.2), and since

$$\lim_{T \rightarrow 0} \frac{m_e - \varepsilon_F}{T} \rightarrow -\infty \quad (3.7)$$

we find

$$C_V^e \simeq 2g(\varepsilon_F) T \int_0^{\infty} \left( \frac{x}{2} \right)^2 \operatorname{sech}^2 \left( \frac{x}{2} \right) dx \quad (3.8)$$

$$\simeq \frac{\pi^2}{3} g(\varepsilon_F) T \quad (3.9)$$

Finally,

$$C_V^e \simeq \frac{\mu_e T}{3} \sqrt{\mu_e^2 - m_e^2} \quad (3.10)$$

Hence, we notice that a relativistic electron gas has a heat capacity at low temperatures that

depends linearly on the temperature.

### B. Electrons at $B \neq 0$

Similarly to the zero-magnetic-field case, we have that in the presence of a constant and uniform magnetic field, the statistical part of the electron thermodynamic potential is given by [7]

$$\Omega_{\beta}^e = -\frac{eB}{4\pi^2\beta} \int_{-\infty}^{\infty} dp \sum_{n=0}^{\infty} d(n) \left[ \ln(1 + e^{-\beta(\varepsilon_n + \mu_e)}) + \ln(1 + e^{-\beta(\varepsilon_n - \mu_e)}) \right], \quad (3.11)$$

Here, the energy spectrum is given by  $\varepsilon_n^2 = p^2 + 2|eB|n + m_e^2$  and the degeneracy is  $d(n) = 2 - \delta_{n0}$  where  $n \in \mathbb{Z}_0^+$  is the Landau level number.

In the low-temperature limit, the leading contribution of Eq. (3.11) will come solely from the particles in the lowest Landau level (LLL), then we have

$$\Omega_{(\beta-LLL)}^e \simeq -\frac{eB}{4\pi^2\beta} \int_{-\infty}^{\infty} \ln(1 + e^{-\beta(\varepsilon_0 - \mu_e)}) dp \quad (3.12)$$

Making a variable change from momentum to energy, we find that

$$\Omega_{(\beta-LLL)}^e \simeq -\frac{2}{\beta} \int_{m_e}^{\infty} d\varepsilon_0 g_B(\varepsilon_0) \ln[1 + e^{-\beta(\varepsilon_0 - \mu_e)}] \quad (3.13)$$

Where

$$g_B(\varepsilon_0) = \frac{eB\varepsilon_0}{4\pi^2 \sqrt{\varepsilon_0^2 - m_e^2}} \quad (3.14)$$

is the density of state per volume of the LLL. Using Eq. (2.4), we find for the thermodynamic potential (3.13),

$$C_V^e(B) \simeq 2 \int_{m_e}^{\infty} d\varepsilon_0 g(\varepsilon_0) \left( \frac{\varepsilon_0 - \mu_e}{2T} \right)^2 \text{sech}^2 \left( \frac{\varepsilon_0 - \mu_e}{2T} \right) \quad (3.15)$$

In the low-temperature limit, repeating the same steps we did for the  $B = 0$  case, we find

$$C_V^e(B) \simeq 2g(\epsilon_F)T \int_{-\infty}^{\infty} \left(\frac{x}{2}\right)^2 \operatorname{sech}^2\left(\frac{x}{2}\right) dx = \frac{2\pi^2}{3}g(\epsilon_F)T \quad (3.16)$$

Substituting (3.14), for  $\epsilon_0 = \epsilon_F$ , into (3.16) it is obtained

$$C_V^e(B) \simeq \frac{eB\mu_e T}{6\sqrt{\mu_e^2 - m_e^2}} \quad (3.17)$$

In this calculation, we neglected the contribution of the interaction of the magnetic field with the anomalous magnetic moment of the electron, since that contribution is negligible for both strong and weak fields [41].

Considering  $\mu_e > m_e$  (see Section 2.2) we can approximate the heat capacity of the electron in the presence of a magnetic field as

$$C_V^e(B) \simeq \frac{eBT}{6} \quad (3.18)$$

Notice that the heat capacity in this low-temperature limit also linearly depends on the temperature, but now it is also proportional to the magnetic field.

### 3.1.2 Heat Capacity of a Nonrelativistic Superfluid of Neutrons

From attractive pion exchanges, neutrons near the Fermi surface can form pairs that can produce boson condensate at the low-temperature limit. Since neutrons don't have electric charge, the pair condensates will keep the neutrality of the ground state, therefore we will observe a macroscopic superfluid state. Similarly, since protons does have charge, their Cooper pairs condensates will create a macroscopic superconductor state. Finally, if the baryonic chemical potential isn't considerably higher than the neutron mass we can use a nonrelativistic approximation in order to find the heat capacity.

Following Landau's calculations in Refs. [42, 43], the thermodynamic potential for a non-relativistic superfluid, treated as an ideal Bose gas formed by the thermally excited quasiparticles, is given by

$$\Omega_{\beta}^n = \frac{1}{\beta} \int \frac{d^3 p}{(2\pi)^3} \ln \left( 1 - e^{-\beta \varepsilon_n} \right) \quad (3.19)$$

with a gapped energy spectrum,

$$\varepsilon_n = \frac{(p - p_0)^2}{2m} + \Delta \quad (3.20)$$

Where  $\Delta$  is the energy gap created by the neutron-pair condensates, and  $p_0$  is the gap location in momentum space.

Performing the same steps we did to get the heat capacity of the electron gas, we substitute Eq. (3.19) into Eq. (2.4), to find

$$C_V^n = \frac{1}{2\pi^2 T^2} \int_0^{\infty} dp p^2 e^{(-\varepsilon_n/T)} \varepsilon_n^2 \quad (3.21)$$

Using the energy spectrum (3.20) in Eq. (3.21), we find

$$C_V^n = \frac{e^{-(\Delta/T)}}{2\pi^2 T^2} \int_0^{\infty} dp p^2 e^{-(p-p_0)^2/2mT} \left( \Delta + \frac{(p-p_0)^2}{2m} \right)^2 \quad (3.22)$$

Doing the variable change  $x = \frac{p-p_0}{\sqrt{2mT}}$ , we can rewrite the heat capacity as

$$C_V^n = \frac{e^{-(\Delta/T)} \sqrt{2mT}}{2\pi^2 T^2} \int_{-\frac{p_0}{\sqrt{2mT}}}^{\infty} dx \left[ p_0^2 + 2x\sqrt{2mT}p_0 + 2mTx^2 \right] e^{-x^2} (\Delta + x^2 T)^2, \quad (3.23)$$

Which in the low-temperature limit can be simplified to

$$C_V^n \simeq \frac{e^{-(\Delta/T)} \sqrt{2m} p_0^2 \Delta^2}{2\pi^2 T^{\frac{3}{2}}} \int_{-\infty}^{\infty} dx e^{-x^2} \quad (3.24)$$

Where higher-order terms in  $\frac{T}{\Delta}$  were neglected.

Finally,

$$C_V^n \simeq \frac{e^{-(\Delta/T)} \Delta^2}{T^{\frac{3}{2}}} \sqrt{\frac{m}{2\pi^3}} p_0^2 \quad (3.25)$$

From Eq. (3.25), we can see the known result that the  $C_V$  of superfluids is exponentially damped by the gap.

The effects on neutrons of the magnetic fields up to  $10^{18}G$  are negligible, as it was shown in Refs. [4, 5]. In the next section, 3.2, we will show that in color superconductivity although the gap is neutral with respect to the rotated electromagnetism, we have significant changes coming from the inner composition made of charged quarks.

### 3.1.3 Heat Capacity of Superfluid Phonons

From Goldstone's theorem we know that when a global symmetry of the Lagrangian or Hamiltonian that describes the system, is spontaneously broken this implies the existence of Goldstone fields. For a superfluid of neutrons at  $T \leq T_c = 10^{10}K$ , we have a new contribution from collective modes generated as massless Goldstone modes associated with the breaking of the baryonic symmetry produced by the condensation of the s-wave neutron Cooper pairs. Those collective modes are known as superfluid phonons.

The phonon heat capacity was calculated in Ref. [44], and it is given by

$$C_V^{(sPh)} = \frac{2\pi^2 T^3}{15v_s^3}, \quad (3.26)$$

where  $v_s \simeq \frac{k_{Fn}}{\sqrt{3M}}$ ,  $M$  is the neutron mass and  $k_{Fn}$  the neutron Fermi momentum. At low temperature, the phonon heat capacity has a cubic dependence on the temperature. Hence, at low temperatures, the electron contribution  $C_V^e$  (see Eq. (3.10)), is larger than that of the superfluid phonons written above in Eq. (3.26). Hence, the electron contribution to CV is the dominant one.

But, once we have an applied magnetic field with a strength  $B \geq 10^{13}G$ , the contribution from phonons becomes larger than that of the electrons in the direction of the transverse to the

field, see Ref. [44]. This is due to the fact that in the presence of a magnetic field the electron heat transport is very anisotropic with the electron motion in the transverse direction limited by the Landau quantization, while the phonons, being neutral, can equally move along and transverse to the field directions.

Increasing the density, the s-wave interactions between neutrons become repulsive, while the attractive p-waves, which produce spin-1 Cooper pairs, are favored as seen in Ref. [45, 46]. Such condensate breaks rotational and baryonic symmetries and give rise to two gapless Goldstones, or *angulons*, associated with the breaking of the rotational symmetry with respect to the two perpendicular axis to the condensate spin direction and to an extra Goldstone, the superfluid phonon. Each of the Goldstone modes give similar contribution to the heat capacity as in Eq. (3.26).

### 3.2 Heat Capacity of Neutron Stars at High Density

At sufficient high densities we expect to observe deconfined quarks and, if the density is larger than the mass of the s quark, the CFL phase will be favored Ref. [47]. In this section we will calculate the heat capacity of the relevant contributions of this CFL phase Ref. [48], first in a system without magnetic field, and latter, in a system with magnetic field which will form the magnetic CFL, also known as the MCFL phase Ref. [49, 50, 51, 52].

#### 3.2.1 Heat Capacity of quark matter in the CFL phase

In the CFL phase, the temperature-dependent thermodynamic potential was found in Ref. [48] as

$$\Omega_{\beta}^{CFL} = -\frac{1}{2\pi^2\beta} \sum_{i=1}^4 \int_0^{\Lambda} dp p^2 \ln[1 + e^{-\beta|\varepsilon_i|}], \quad (3.27)$$

with energy spectra given by

$$|\varepsilon_{1,2}| = \sqrt{(p \mp \mu)^2 + \Delta^2}, \quad |\varepsilon_{3,4}| = \sqrt{(p \mp \mu)^2 + 4\Delta^2} \quad (3.28)$$



where  $\Delta$  is the CFL gap,  $\mu$  is the baryonic chemical potential and  $\Lambda$  is the momentum cutoff of the low-energy theory described by a Nambu–Jona-Lasinio (NJL) model [47]. Once again, substituting the thermodynamic potential Eq. (3.27) into Eq. (2.4), we find that the heat capacity is given by

$$C_V^{CFL} = \frac{1}{2\pi^2 T^2} \sum_{i=1}^4 \int_0^\Lambda dp p^2 \varepsilon_i^2 \operatorname{sech}^2 \left( \frac{|\varepsilon_i|}{2T} \right) \quad (3.29)$$

Which can be rewritten as

$$C_V^{CFL} = \frac{2T^3}{\pi^2} \sum_{i=1}^4 \int_0^{\hat{\Lambda}} dx x^2 \hat{\varepsilon}_i^2 \operatorname{sech}^2 \left( \frac{|\hat{\varepsilon}_i|}{2} \right) \quad (3.30)$$

where  $x = \frac{p}{T}$  and  $\hat{Q} = \frac{Q}{T}$  for all the quantities, including  $|\hat{\varepsilon}_{1,2}| = \sqrt{(x \mp \hat{\mu})^2 + \hat{\Delta}^2}$  and  $|\hat{\varepsilon}_{3,4}| = \sqrt{(x \mp \hat{\mu})^2 + 4\hat{\Delta}^2}$ .

In the low-temperature limit, the leading contribution in Eq. (3.30) can be expressed as

$$C_V^{CFL} \simeq \frac{2T^3}{\pi^2} \sum_{i=1}^4 \int_0^{\hat{\Lambda}} dx x^2 \hat{\varepsilon}_i^2 \exp(-|\hat{\varepsilon}_i|) \quad (3.31)$$

Because of the negative exponential,  $\exp(-|\hat{\varepsilon}_i|)$ , the main contribution in Eq. (3.31) comes from the region around the integral lower limit. Thus, up to a numerical coefficient, we can extract the leading contribution making

$$C_V^{CFL} \simeq \left[ \frac{(\mu^2 + \Delta^2)T}{\pi^2} e^{-\frac{\sqrt{\mu^2 + \Delta^2}}{T}} + \frac{(\mu^2 + 4\Delta^2)T}{\pi^2} e^{-\frac{\sqrt{\mu^2 + 4\Delta^2}}{T}} \right] \int_0^1 dx x^2 \quad (3.32)$$

Finally, we have

$$C_V^{CFL} \simeq \frac{(\mu^2 + \Delta^2)T}{3\pi^2} e^{-\frac{\sqrt{\mu^2 + \Delta^2}}{T}} + \frac{(\mu^2 + 4\Delta^2)T}{3\pi^2} e^{-\frac{\sqrt{\mu^2 + 4\Delta^2}}{T}} \quad (3.33)$$

Hence, we obtain that in this case, similar to the superfluid state, the heat capacity is exponentially

damped at low temperature, with a damping factor that depends on the gap and baryonic chemical potential.

### 3.2.2 Heat Capacity of Goldstone modes in the CFL phase

Taking into account that the symmetry-breaking pattern in the CFL is given by (see Ref. [53, 54, 55]),

$$\mathcal{G} = SU(3)_C \times SU(3)_L \times SU(3)_R \times U(1)_A^{(1)} \times U(1)_B \rightarrow SU(3)_{C+L+R}. \quad (3.34)$$

This symmetry reduction leaves ten Goldstone bosons: a singlet associated with the breaking of the baryonic symmetry  $U(1)_B$ , another singlet associated with the breaking of the  $U(1)_A^{(1)}$  approximated symmetry (The group  $U(1)_A^{(1)}$ , not to be confused with the usual anomaly  $U(1)_A$ , is related to the current which is an anomaly-free linear combination of  $s$ ,  $d$ , and  $u$  axial currents [56]), and an octet associated with the axial  $SU(3)_A$  group.

If the baryonic chemical potential is not sufficiently large to justify neglecting the quark masses, the breaking of the axial  $SU(3)_A$  group is only apparent. If this is the case then we have an octet of massive pseudo-Goldstone modes associated with the breaking of the global symmetry  $SU(3)_A$ , another pseudo-Goldstone associated with the breaking of the  $U(1)_A^{(1)}$  group and only one massless Goldstone mode associated with the breaking of the baryonic symmetry. The corresponding  $C_V$ 's of the massive and massless modes were found in Ref. [57] and are given, respectively, by

$$C_V^B \simeq \frac{m^{7/2}}{2\sqrt{2}\pi^{3/2}v^3\sqrt{T}} e^{-\frac{m}{T}} \quad (3.35)$$

and

$$C_V^G = \frac{2\pi^2 T^3}{15v^3} \quad (3.36)$$

In these equations,  $m$  is the mass of the pseudo-Goldstones and  $v$  is their velocity, which should be

found from the CFL microscopic theory. Comparing Eq. (3.36) with Eq. (3.33) and Eq. (3.35), we can confirm that the major contribution in the CFL phase comes from the massless Goldstones.

### 3.2.3 Heat Capacity of quark matter in the MCFL phase

As said in the beginning of Section 3.2, for high density limits and in the presence of a magnetic field we have a new phase called MCFL Ref. [50, 51, 52] which sees a reduction in symmetries when compared to the CFL phase, because a magnetic field interacting with quarks of different electric charges reduces the flavor symmetry and it also breaks rotational symmetry.

Furthermore, in this color superconducting phase we need to redefine electromagnetism. Though the original electromagnetic  $U(1)_{em}$  symmetry is broken by the formation of quark Cooper pairs that are electrically charged Ref. [58], a residual  $\tilde{U}(1)$  symmetry still remains Ref. [23]. The massless gauge field associated with this symmetry is given by the linear combination of the conventional photon field and the eight-gluon field Ref. [23, 59, 60],  $\tilde{A}_\mu = \cos \theta A_\mu - \sin \theta G_\mu^8$ , with the mixing angle given as a function of the strong coupling constant  $g$  and the electromagnetic coupling  $e$  as  $\theta = \cos^{-1} \left( g \sqrt{e^2/3 + g^2} \right)$ . The field  $\tilde{A}_\mu$  works as an in-medium or rotated electromagnetic field. Therefore, a magnetic field associated with  $\tilde{A}_\mu$  can penetrate the color superconductor without being subject to the Meissner effect, since the color condensate is neutral with respect to the corresponding rotated electric charge. In this phase, the temperature-dependent part of the thermodynamic potential of this phase can be written as Ref. [61]

$$\Omega_\beta^{MCFL} = \Omega_C + \Omega_N, \quad (3.37)$$

where

$$\Omega_C = -\frac{\tilde{e}\tilde{B}}{4\pi^2\beta} \sum_{n=0}^{\infty} d(n) \sum_{i=1}^2 \int_0^\Lambda dp \ln \left( 1 + e^{-\beta|\varepsilon_i^{(c)}|} \right) \quad (3.38)$$

is the contribution of the rotated-charged quarks,  $n \in \mathbb{Z}_0^+$  is the Landau level number and  $\tilde{B}$ . Simi-

larly,  $\Omega_N$  is the contribution from the rotated-neutral quarks, which is simply

$$\Omega_N = -\frac{1}{4\pi^2\beta} \sum_{i=1}^6 \int_0^\Lambda dp p^2 \ln \left( 1 + e^{-\beta|\varepsilon_i|} \right) \quad (3.39)$$

The energy spectra in these equations are given by

$$|\varepsilon_{1,2}^{(c)}| = \left[ \left( \sqrt{p^2 + 2\tilde{e}\tilde{B}n \pm \mu} \right)^2 + \Delta_H^2 \right]^{1/2} \quad (3.40)$$

$$|\varepsilon_{1,2}^{(0)}| = \sqrt{(p \pm \mu)^2 + \Delta^2}, \quad |\varepsilon_{3,4}^{(0)}| = \sqrt{(p \pm \mu)^2 + \Delta_a^2}, \quad |\varepsilon_{5,6}^{(0)}| = \sqrt{(p \pm \mu)^2 + \Delta_b^2} \quad (3.41)$$

with

$$\Delta_a = \frac{1}{2} \left[ \Delta + \sqrt{\Delta^2 + 8\Delta_H^2} \right] \quad \Delta_b = \frac{1}{2} \left[ \Delta - \sqrt{\Delta^2 + 8\Delta_H^2} \right] \quad (3.42)$$

In the expressions above  $\Delta$  and  $\Delta_H$  denote the two gaps of the MCFL phase Ref. [50, 51, 52]. Here, since this phase lowers the system symmetry, it doubles the number of gaps as compared with the CFL phase. As a consequence of the breaking of rotational symmetry by the uniform magnetic field, which opens new interaction channels, a third gap appears related to the interaction of the magnetic field with the anomalous magnetic moment of the diquark pairs as studied in Ref. [62]. This new gap can be neglected at moderate magnetic fields, but it becomes significant when  $B \gtrsim 10^{19} G$ .

From Eq. (2.4) we can check that for  $\Omega_N$  the result is exponentially damped at low temperatures, similarly to the CFL case, Eq. (3.33). In the case of  $\Omega_C$ , in the low-temperature limit, the leading contribution to  $C_V$ , comes from the LLL because of the negative exponential term in Eq. (3.38). Therefore, we can approximate

$$\Omega_C^{(LLL)} \simeq -\frac{\tilde{e}\tilde{B}}{4\pi^2\beta} \sum_{i=1}^2 \int_0^\Lambda dp \ln \left( 1 + e^{-\beta|\varepsilon_i^{(LLL)}|} \right) \quad (3.43)$$

with

$$|\varepsilon_{1,2}^{(LLL)}| = \sqrt{(p \pm \mu)^2 + \Delta_H^2} \quad (3.44)$$

From Eq. (3.43), we obtain the heat capacity

$$C_V^{MCFL} = -\frac{\tilde{e}\tilde{B}}{16\pi^2 T^2} \sum_{i=1}^2 \int_0^\Lambda dp |\hat{\varepsilon}_i|^2 \operatorname{sech}^2 \left( \frac{|\hat{\varepsilon}_i|}{2T} \right), \quad (3.45)$$

where we are using, once again, the notation  $\hat{Q} = \frac{Q}{T}$  for all physical quantities. The equation above can be simplified in the low-temperature limit as

$$C_V^{MCFL} \simeq \frac{\tilde{e}\tilde{B}}{4\pi^2 T^2} \sum_{i=1}^2 \int_0^\Lambda dp |\varepsilon_i|^2 e^{-|\varepsilon_i|/T} \quad (3.46)$$

Defining a new variable  $x := \frac{p}{T}$  and considering that  $\mu > p$ , we obtain

$$C_V^{MCFL} \simeq \frac{\tilde{e}\tilde{B}T}{2\pi^2} \int_0^1 (\hat{\mu}^2 + \hat{\Delta}_H^2) e^{-\sqrt{\hat{\mu}^2 + \hat{\Delta}_H^2}} dx \quad (3.47)$$

and finally after integration

$$C_V^{MCFL} \simeq \frac{\tilde{e}\tilde{B}}{2\pi^2 T} (\mu^2 + \Delta_H^2) e^{-\sqrt{\mu^2 + \Delta_H^2}/T} \quad (3.48)$$

Comparing Eq. (3.48) with Eq. (3.33), we see that the MCFL heat capacity is larger at low temperature than that of the CFL phase, although it is also exponentially damped by the baryonic chemical potential and the gap formed by quarks that are charged with respect to the electromagnetism inside the superconductor.

### 3.2.4 Heat Capacity of Goldstone modes in the MCFL phase

As we already know the MCFL phase presents a different symmetry-breaking pattern than that of the CFL phase. In fact, if a system has a magnetic field, the difference between the electric

charge of the  $u$  quark and that of the  $d$  and  $s$  quarks reduces the original flavor symmetry of the theory, and consequently also the symmetry group remaining after the diquark condensate is formed. Then, the breaking pattern for the MCFL-phase Ref. [50, 51, 52] becomes

$$\mathcal{G}_{\mathcal{B}} = SU(3)_C \times SU(2)_L \times SU(2)_R \times U(1)_A^{(1)} \times U(1)_B \rightarrow SU(2)_{C+L+R} \quad (3.49)$$

The magnetic field applied to the superconducting phase reduces the number of Goldstone bosons, from nine to only five, three of them related to the breaking of  $SU(2)_A$ , one to the breaking of  $U(1)_A^{(1)}$ , and one to the breaking of  $U(1)_B$ . Another characteristic of the MCFL phase, besides the reduction of Goldstone fields, is that all these bosons are neutral with respect to the rotated electric charge Ref. [63]. Thus, no charged low-energy excitation can be produced in the MCFL phase.

Therefore, we can say that once the magnetic field is present, the original symmetry group  $\mathcal{G}$  is reduced, to  $\mathcal{G}_{\mathcal{B}}$ , and that the low energy theory should immediately correspond to the breaking pattern (Eq. 3.49), having only five neutral Goldstone bosons. However, at very weak magnetic fields the symmetry of the CFL phase can be treated as a good approximated symmetry, meaning that at weak fields the low-energy excitations are essentially governed by ten approximately massless scalars (those of the breaking pattern Eq. (3.34)) instead of five. From there, we can understand what is the threshold-field strength that effectively separates the CFL low-energy behavior from the MCFL one.

In fact, the threshold field that marks the reduction in the number of Goldstones was found in Ref. [63]. First, we recall that when a magnetic field interacts with a charged particle, it endows it with an effective mass. Now, in order to have a stable meson in this medium, its mass must be less than twice the gap, otherwise it will decay into a particle-antiparticle pair. Hence, for an effective transition between the CFL  $\rightarrow$  MCFL symmetries, there must be a threshold field, which in Ref. [63] was found to be of order  $10^{16}G$ .

In the MCFL phase, where only neutral Goldstone bosons exist, four massive (their masses

don't depend on the magnetic field) and one massless (associated with the baryonic symmetric breaking), we have that the corresponding heat capacities are expressed by similar formulas to Eq. (3.35) and Eq. (3.36), respectively. Therefore, the contribution from the Goldstone mode associated with the breaking of the baryonic symmetry is the dominant one for the heat capacity in the MCFL phase.

### 3.3 Heat Capacity of Neutron Stars at Intermediate Density

From QCD-inspired NJL models we know that, with increasing chemical potential, the energy separation between quarks and anti-quarks increases, so that it is not energetically favorable to excite anti-quarks from the Dirac sea to be paired with quarks at the Fermi surface. Since the densities aren't high enough we don't expect to observe a CFL phase and, therefore, we need to consider different matter phases in such case. Either no condensate is favored, and the chiral symmetry is restored, or quarks and holes near the Fermi surface pair with parallel momenta and we have inhomogeneous chiral condensates. Finally, quarks may pair with quarks forming a color superconductor phase, which will be, in general, inhomogeneous at the moderate densities we are working with Ref. [64, 65]. The last two possibilities are usually favored Ref. [64, 65, 66, 33], meaning that the transition to a chirally restored phase found in NJL models with increasing density [67] will most likely occur in more than one step, or perhaps will not occur.

As mentioned in the Introduction, we will calculate the heat capacity of one of the inhomogeneous chiral condensate phase, known as the MDCDW phase, that is formed precisely at intermediary densities in the presence of a magnetic field [66]. A magnetic field appears naturally in a NS and it is essential in order to maintain the stability of this phase which indicates that it is plausible to appear inside its core. Furthermore, we are interested in this phase because it is compatible with various astrophysical constraints as seen in Ref. [68] and it presents interesting anomalous electromagnetic transport properties [32, 69].

### 3.3.1 Heat Capacity of quark matter in the MDCDW phase

The temperature-dependent thermodynamic potential for this phase is given by [66]

$$\Omega_{\beta}^{MDCDW} = - \sum_{f=u,d} \frac{|e_f B| N_c}{(2\pi)^2 \beta} \int_{-\infty}^{\infty} dp \sum_{l, \xi, \varepsilon} \ln \left( 1 + e^{-\beta(|E_{l, \xi, \varepsilon}^f - \mu|)} \right) \quad (3.50)$$

where  $N_c$  is the color number,  $f$  denotes the flavor index for quarks  $u$  and  $d$ ,  $l$  is the Landau level number, and the energy spectra are given by

$$\begin{aligned} E_{0, \varepsilon} &= \varepsilon \sqrt{m^2 + p^2} + b, \quad \varepsilon = \pm, l = 0 \\ E_{l, \xi, \varepsilon}^f &= \varepsilon \left[ \left( \xi \sqrt{m^2 + p^2} + b \right)^2 + 2|e_f B| l \right]^{1/2}, \quad \varepsilon = \pm, \xi = \pm, l = 1, 2, 3, \dots \end{aligned} \quad (3.51)$$

In Eq. (3.51),  $m$  and  $b$  are respectively the amplitude and modulation of the inhomogeneous condensate. These are dynamical parameters and can be found through the system gap equations as shown in Refs. [33, 66]. Also, from (3.51) we can see that the energy spectrum is asymmetric in the LLL around the zero-energy level, this asymmetry has topological implications which were discussed in Refs. [32, 69, 70]

Substituting Eq. (3.50) in Eq. (2.4), we find

$$C_V^{MDCDW} = \sum_{f=u,d} \frac{|e_f B| N_c}{(2\pi)^2} \sum_{l, \xi, \varepsilon} \int_{-\infty}^{\infty} dp \left( \frac{|E_{l, \xi, \varepsilon}^f - \mu|}{2T} \right)^2 \operatorname{sech}^2 \left( \frac{|E_{l, \xi, \varepsilon}^f - \mu|}{2T} \right) \quad (3.52)$$

Which, in the low-temperature limit, can be approximated to

$$C_V^{MDCDW} \simeq \sum_{f=u,d} \frac{4|e_f B| N_c}{(2\pi)^2} \sum_{l, \xi, \varepsilon} \int_{-\infty}^{\infty} dp \left( \frac{|E_{l, \xi, \varepsilon}^f - \mu|}{2T} \right)^2 e^{-|E_{l, \xi, \varepsilon}^f - \mu|/T} \quad (3.53)$$

Once again, we have a negative exponential so that the leading contribution comes from the LLL, and from  $\varepsilon = -$  because of the modulus in the exponent. Now, we can express the heat



capacity as

$$C_V^{MDCDW} \simeq \sum_{f=u,d} \frac{2|e_f B|N_c}{(2\pi)^2} \int_0^\infty dp \left( \frac{|E_{0,-}^f - \mu|}{2T} \right)^2 \text{sech}^2 \left( \frac{|E_{0,-} - \mu|}{2T} \right) \quad (3.54)$$

$$\begin{aligned} &= \sum_{f=u,d} \frac{2|e_f B|N_c}{(2\pi)^2} \\ &\times \int_0^\infty dp \left( \frac{|-\sqrt{p^2 + m^2} + b - \mu|}{2T} \right)^2 \text{sech}^2 \left( \frac{|-\sqrt{p^2 + m^2} + b - \mu|}{2T} \right) \end{aligned} \quad (3.55)$$

Now, making the variable change  $p/T \rightarrow p'$ , we have

$$\begin{aligned} C_V^{MDCDW} &\simeq \sum_{f=u,d} \frac{2|e_f B|N_c T}{(2\pi)^2} \\ &\times \int_0^\infty dp' \left( \frac{|-\sqrt{p'^2 + \hat{m}^2} + \hat{b} - \hat{\mu}|}{2} \right)^2 \text{sech}^2 \left( \frac{|-\sqrt{p'^2 + \hat{m}^2} + \hat{b} - \hat{\mu}|}{2} \right) \end{aligned} \quad (3.56)$$

Where we used the normalization notation  $\hat{Q} = Q/T$  in Eq. (3.57).

Introducing the new variable change

$$x := -\sqrt{p'^2 + \hat{m}^2} + \hat{b} - \hat{\mu} = \hat{E}_{0,-} - \hat{\mu} \quad (3.57)$$

with

$$dp' = \frac{x - \hat{b} + \hat{\mu}}{\sqrt{(x - \hat{b} + \hat{\mu})^2 - \hat{m}^2}} dx \quad (3.58)$$

we obtain

$$C_V^{MDCDW} \simeq \sum_{f=u,d} 2N_c T \int_{\hat{m} + \hat{b} - \hat{\mu}}^\infty dx g_f(x) \left( \frac{|x|}{2} \right)^2 \text{sech}^2 \left( \frac{|x|}{2} \right) \quad (3.59)$$

where  $g_f(x)$  represents the system density of states per unit volume given by

$$g_f(x) = \frac{|e_f B|}{4\pi^2} \frac{x - \hat{b} + \hat{\mu}}{\sqrt{(x - \hat{b} + \hat{\mu})^2 - \hat{m}^2}} \quad (3.60)$$

As it was discussed in Section 3.1.1, the Fermi-Dirac distribution at low temperature only changes significantly in the vicinity of the Fermi energy. Similarly, the integral in Eq. (3.59) main contributions comes from the surroundings of  $E_{0,-} = \mu$ . From Eq. (3.60) we see that  $g_f(E_{0,-} = \mu) \equiv g_f(x=0)$  which enables us to write the density of states  $\hat{g}_f(x)$  as  $\hat{g}_f(x=0)$ . After this change and taking into account that in the  $T \rightarrow 0$  limit the lower limit in the integral of Eq. (3.59) goes to negative infinity because  $\mu > m, b$ , we find

$$\begin{aligned}
C_V^{MDCDW} &\simeq 2N_c T \sum_{f=u,d} g_f(0) \int_{-\infty}^{\infty} \left(\frac{x}{2}\right)^2 \operatorname{sech}^2\left(\frac{x}{2}\right) dx \\
&\simeq \frac{2\pi^2 N_c}{3} T \sum_{f=u,d} g_f(0) \\
&\simeq \frac{(\mu - b)|eB|T}{2\sqrt{(\mu - b)^2 - m^2}} \tag{3.61}
\end{aligned}$$

Here, we have neither a superfluid phase nor a superconducting phase and we can observe that the heat capacity isn't so damped as in the CFL phase found in Subsection 3.2.1, which had a negative exponential damping. The  $C_V$  in this case depends on the dynamical parameters  $m$  and  $b$  that have to be determined by the system gap equations, as mentioned. These parameters will decrease with the temperature, but even if  $T = 0$ , we have that  $\mu > b > m$  in the region of interest [63, 66]. Hence,  $C_V^{MDCDW} \sim eBT/2$ .

If we compare Eq. (3.17) after neglecting  $m_e$ , with Eq. (3.61) after neglecting  $m$  and  $b$ , we see that the quark contribution to the heat capacity is 3 times larger than the electron contribution at the same temperature and with the same magnitude of the magnetic field. This is due to the quark phase having more degrees of freedom, specially the three color degrees of freedom, because the flavor ones enter in  $C_V$  through  $|e_f B|$ , hence the fractional quark charges in the flavor sum gives  $|eB|$  without an extra factor.

It is important to notice that at intermediate densities, other phases can compete with the

MDCDW phase. With decreasing densities homogeneous CS phases, such as CFL and the 2SC, become gapless and unstable [24, 25, 71, 72]. This instability manifests itself through imaginary Meissner masses for some of the gluons which indicates an instability towards spontaneous breaking of translational invariance [26, 27, 28, 29]. This means that inhomogeneous phases will be also favored in color superconductivity.

Most inhomogeneous CS phases are based on the idea of Larkin and Ovchinnikov (LO) [73] and Fulde and Ferrell [74], originally applied to condensed matter. In the CS LOFF phases [75, 76, 77], quarks of different flavors form Cooper pairs with nonzero momentum. CS inhomogeneous phases with gluon condensates that break rotational symmetry [78] have also been considered to solve the chromomagnetic instability, we expect these phases to have larger  $C_V$  values but their calculations are a pending task.

### 3.4 Heat Capacity Estimates for Different Neutron Star Compositions

In this section we want to estimate the main contributions to the heat capacity from different phases that were discussed in previous sections and then to compare the contributions with the phenomenological constraint  $\tilde{C}_V \gtrsim 10^{36} (T/10^8) \frac{\text{erg}}{\text{K}}$  coming from astrophysical observations. This will give us important informations such as, which phases respect the constraint and therefore, are feasible to appear inside NS and which are the ones given a major contribution.

#### 3.4.1 Nuclear Matter Phase

The low density limit for NS is completely dominated by nuclear matter, i.e, neutrons, protons and electrons which will give the main contribution to the heat capacity. If neutron and protons are in superfluid and superconducting states respectively, their contributions to  $C_V$  can be neglected, as commented before. Therefore, the main contribution comes from unpaired neutrons and electrons. We will try to estimate the order of these contributions for a NS in the absence and in the presence of the magnetic field.

##### A. Unpaired Neutrons

We can find the heat capacity for neutrons with similar steps we did for electrons, we just have to substitute  $\mu_e$  by the baryonic chemical potential  $\mu$ , and the electron mass by the neutron mass  $m_n$ , so that from Eq. (3.10), we find

$$C_V^n \simeq \frac{\mu T}{3} \sqrt{\mu^2 - m_n^2} \quad (3.62)$$

From QCD we know that a single particle density  $n$  is given in terms of the Fermi momentum by

$$n = \frac{d}{6\pi^2} k_F^3 \quad (3.63)$$

where  $d$  counts the internal degrees of freedom. Therefore for  $d = 2$  (spin degeneracy) the Fermi momentum can be written as

$$k_F = c\hbar (3\pi^2 n_N)^{1/3} \quad (3.64)$$

If  $n_B = 3n_s$  and  $n_N \simeq n_B$ , where  $n_s = 0.15\text{fm}^{-3}$  is the saturation density. The baryonic chemical potential can be written as

$$\mu = \sqrt{k_F^2 + m_n^2} \quad (3.65)$$

where  $m_n \simeq 939.57$  MeV is the neutron mass. Therefore, from Eq.(3.64) we can calculate the Fermi momentum, then we find  $\mu = 1050$  MeV and the corresponding Fermi temperature  $T_F = \frac{\mu}{k_B} \simeq 12.2 \times 10^{12} K$ .

If  $\mu > m_n$ , the heat capacity Eq. (3.62) can be simplified as

$$C_V^N \simeq \frac{\mu^2 k_B^2 T}{3}, \quad (3.66)$$

here we included  $k_B^2$ , associated with the second derivative with respect to the temperature  $T$  in Eq. (2.4) (Notice that, on the other hand, in the thermodynamic potential,  $T$ , appears always multiplied by  $k_B$ ). We can approximate the neutron number density by  $n_N = \frac{2\mu^3}{3\pi^2}$  and, from the Fermi

temperature  $k_B T_F = \mu$ , we can rewrite Eq. (3.66) as

$$C_V^N \simeq \frac{\pi^2}{2} n_N k_B \left( \frac{T}{T_F} \right) \quad (3.67)$$

Finally, for  $n_N = 3n_s$  and  $T_F = 12.2 \times 10^{12} \text{K}$ , choosing  $T = 10^8 \text{K}$ , we obtain the volumetric heat capacity

$$C_V^N \simeq 0.25 \times 10^{19} \frac{\text{erg}}{\text{K cm}^3} \quad (3.68)$$

We can compare the result above with those found in Ref. [79]. In order to do that, first we multiply Eq. (3.68) by the volume of a NS of radius  $R = 10 \text{ km}$ , considering it a perfect sphere, so that  $V_{NS} = \frac{4}{3} \pi R^3 = 4.2 \times 10^{18} \text{cm}^3$ . Although it is a rough approximation, it is useful since we can find the order of the heat capacity for a given temperature, which, in this case, is given by

$$\tilde{C}_V^N = C_V^N \times V_{NS} = 0.1 \times 10^{38} \frac{\text{erg}}{\text{K}}, \quad (3.69)$$

this result is of the same order as the one reported in Ref. [79]. The inclusion of a magnetic field can be done through the anomalous-magnetic-moment/magnetic field interaction. This calculation was performed in Ref. [4, 5] and it was found that up to magnetic fields of  $10^{18} \text{G}$  the magnetic field effect on the heat capacity  $C_V$  is negligible.

The calculations for unpaired protons in a system without magnetic field is similar to what we did in this section. We just need to replace  $n_p = X_e n_N$ , where  $n_p$  and  $n_N$  are the number densities of protons and neutrons, respectively, and  $X_e$  is the electron fraction, which is expected to be larger than a threshold value  $X_e \sim 1/9$  in order for the direct URCA process to occur in NSs Ref. [80]. If  $B \neq 0$ , the calculations are similar to what is reported in Subsection, 3.4.1 - C, with the replacement of the mass  $m_e \rightarrow m_n$  and chemical potential  $\mu_e \rightarrow \mu - \mu_e$ .

## B. Electrons at $B=0$

For  $\mu_e > m_e$ , we rewrite Eq. (3.10) as

$$C_V^e \simeq \frac{\mu_e^2 k_B^2 T}{3}, \quad (3.70)$$

Where, as in Eq. (3.66), we included the square of the Boltzmann constant and neglect  $m_e$  considering that  $\mu_e > m_e$ . From the electron number density  $n_e = 2\mu_e^3/3\pi^2$  and the Fermi temperature  $k_B T_F = \mu_e$ , we can manipulate Eq. (3.70), so that

$$C_V^e \simeq \frac{\pi^2}{2} n_e k_B \left( \frac{T}{T_F} \right) \quad (3.71)$$

Now we want to estimate the electron number density, using electric neutrality we know that  $n_e = n_p = X_e n_N$ . Thus, for  $n_N = 3n_s$ , we have  $n_e = (1/3)n_s$ , with a corresponding  $T_F = 2.1 \times 10^{12} \text{K}$ . Substituting with these values in (3.71), we obtain for  $T = 10^8 \text{K}$  the volumetric heat capacity

$$C_V^e \simeq 0.2 \times 10^{19} \frac{\text{erg}}{\text{K cm}^3} \quad (3.72)$$

Multiplying by the volume for a NS with 10 km radius, as we did for neutrons, we obtain

$$\tilde{C}_V^e = C_V^e \times V_{NS} = 0.8 \times 10^{37} \frac{\text{erg}}{\text{K}}, \quad (3.73)$$

which is of the same order than the one reported in [79]. It is important to notice that for the massless Goldstones  $\tilde{C}_V^G \sim n_s \left( \frac{T}{T_F} \right)^3 \ll \tilde{C}_V^e$  since  $\left( \frac{T}{T_F} \right) \sim 10^{-4}$ .

### C. Electrons at $\mathbf{B} \neq \mathbf{0}$

Considering the same approximation used in the previous section, from Eq. (3.17) we can write

$$C_V^e(B) \simeq \frac{e B k_B^2 T}{6} \quad (3.74)$$

The electron number at zero temperature in this case is given by

$$N^e(B) = -\frac{\partial \Omega_{LLL}^{(e)}}{\partial \mu_e} = \frac{eB}{2\pi^2} \sqrt{\mu_e^2 - m_e^2} \simeq \frac{eB\mu_e}{2\pi^2} \quad (3.75)$$

Here, if the number density of electrons is equal to the one calculated in the  $B = 0$  case, for the same chemical potential, we would need to have a magnetic field  $B = \frac{2\mu^2}{3} = 1.7 \times 10^{19}$  G, which is a value too high to be expected inside the NS core [4, 5].

Multiplying and dividing the right hand side of Eq. (3.74) by  $\mu_e$  and introducing the Fermi temperature as before we have

$$C_V^e(B) \simeq \frac{\pi^2 N_{(LLL)}^{(e)} k_B}{3} \left( \frac{T}{T_F} \right) \quad (3.76)$$

Keeping the same parameters than in the  $B = 0$  case, we obtain

$$\tilde{C}_V^e(B) \simeq 0.2 \times 10^{37} \frac{\text{erg}}{\text{K}}, \quad (3.77)$$

If we consider a realistic field value of  $B \sim 10^{17}$  G, the heat capacity decreases by two orders in relation to  $C_V^{(e)}$ . Hence, we find that in the presence of a moderately high magnetic field  $\sim 10^{17}$  G, the electron heat capacity decreases.

### 3.4.2 Quark Phase

Below, we consider the contribution of quark matter at intermediate densities to the heat capacity of NS, paying special attention to the inhomogeneous MDWD phase.

Here, we are considering a quark star which is formed only by quarks and a small cloud of electrons occupying a region of a few fm around the quark surface [81]. Based on the Bodmer-Terazawa-Witten hypothesis (see Introduction) [15, 16, 17], it is possible that a Neutron Star made up solely of quarks is the most energetically favored configuration once quark matter is present

inside it, i.e. this NS is either formed solely by three-flavor (u, d and s), which is known as a strange star, or two-flavor (u and d) quark matter.

The proposal that a strange star can be stable takes into account the fact that strange matter, which consists of roughly equal numbers of  $u$ ,  $d$ , and  $s$  quarks at high densities is absolutely stable (it has lower energy per baryon than ordinary iron nuclei) which, as said, comes from Bodmer-Terezawa-Witten hypothesis [15, 16, 17]. Recently, it was shown using phenomenological quark-meson model, including flavor-dependent feedback of the quark gas on the QCD vacuum, that  $u$ - $d$  quark matter is in general more stable than strange quark matter, and it can be more stable than ordinary nuclear matter if the baryon number is large enough, above  $A_{min} \gtrsim 300$  which, on the other hand, ensures the stability of ordinary nuclei.

We are going to consider a two-flavor quark star whose interior is made up solely by  $u$  and  $d$  quarks in order to work with the two-flavor MDCDW phase in the section below.

### A. Quarks in the MDCDW phase

As discussed in Section 3.3, at intermediate densities where it is possible to realize the MDCDW phase, the heat capacity given in Eq. (3.61) can be reduced to

$$C_V^{MDCDW} \simeq \frac{eBT}{2} \quad (3.78)$$

From [32, 69], we know that the quark number density for the MDCDW phase is given by

$$n_q = n_{anom} + n_{ord} \quad (3.79)$$

Here  $n_{anom} = 3 \frac{|eB|b}{2\pi^2}$  is the so-called anomalous quark number density, and  $n_{ord} = 3 \frac{|eB|\mu}{2\pi^2}$  is the ordinary contribution coming from the MDCDW non-anomalous many-particle thermodynamic potential at zero temperature. Since  $\mu > b$  in the region of interest, we have that the leading contribution



comes from the nonanomalous part,

$$n_q \simeq n_{ord} = \frac{3|eB|\mu}{2\pi^2} \quad (3.80)$$

Finally, substituting Eq. (3.80) into Eq. (3.78), we find

$$C_V^{MDCDW} \simeq \frac{\pi^2}{3} n_q k_B \left( \frac{T}{T_F} \right) \quad (3.81)$$

To find the order of the contribution of this phase to the heat capacity, we need to find the quark number density, thus we consider that the baryonic number density is  $n_B = 3n_s$ , therefore, the quark number density is  $n_q = \frac{n_B}{3} = n_s$ , and the corresponding Fermi temperature is  $T_F = 2.6 \times 10^{12}$  K. Substituting these quantities in (3.81) we obtain for  $T = 10^8$  K the volumetric heat capacity

$$C_V^{MDCDW} \simeq 0.26 \times 10^{19} \frac{\text{erg}}{\text{K cm}^3} \quad (3.82)$$

In order to find the heat capacity, we multiply this result by the volume of a star of radius 10 km.

$$\tilde{C}_V^{MDCDW} = C_V^N \times V_{NS} = 0.1 \times 10^{38} \frac{\text{erg}}{\text{K}}, \quad (3.83)$$

which is of the same order as the one obtained for unpaired neutrons Eq. (3.69).

## CHAPTER IV

### CONCLUSION

This thesis deals with investigating the dominant contributions to the heat capacity of NS due to the different matter states that can be realized in the stellar core. As is it well known, depending on the baryonic density that can be reached in the core and on the value of the existing magnetic field, different states of matter will prevail. Our focus, in particular, is to check, based on this thermodynamical study associated to the different media heat capacity, if deconfined quark matter can play a role in the star's inner composition. We pay special attention to the thermal properties of a new quark-matter phase called the Magnetic Dual Chiral Density Wave phase that can be realized in the intermediate density regime that can be the more appropriate one inside this compact objects.

Our work consists in deriving from first principles of statistical mechanics, the heat capacity of different dense matter phases comparing the results with the one obtained from astrophysical observations. Observing NSs after the accretion outburst help us to comprehend the crust heat capacity [82, 83, 84], and long-running observations on a timescale of years can give us limiting values of the heat capacity of NSs core. A lower limit to the heat capacity was found from those observations to be  $C_V \gtrsim 10^{36} \left(\frac{T}{10^8}\right) \frac{\text{erg}}{\text{K}}$  [79]. Our calculations indicate that matter states that exhibit superfluidity or superconductivity do not satisfy this constraint, since in those cases  $C_V$  is exponentially damped. At low densities, only electron-rich media and those with a large number of unpaired neutrons have heat capacities satisfying the constraint. At high densities the situation is different. If we consider that the most favorable quark-matter state at those very high densities and in the presence of a magnetic field is the color superconducting phase known as the magnetic color-

flavor-locking (MCFL) phase, since being a superconducting phase does not satisfy the minimum constraint for the heat capacity, so invalidating the presence of quark matter in the core. But as we already discussed, the densities inside a NS core aren't asymptotically high enough to make the MCFL reliable and we should look for other phases that are more suitable at intermediate densities.

For feasible intermediate densities which are expected to be reached in the inner core of a NS, other phases can be realized [85]. Good candidates for quark-matter phases at the intermediate densities and low temperatures found in the NS's core are the chiral inhomogeneous condensate phases formed by particle-hole pairs, and in particular the phase known as MDCDW that we consider in this thesis. Considering the MDCDW phase, we prove that the heat capacity for this phase has the same behavior as the heat capacity of media formed by electrons and unpaired neutrons, i.e, it is a linear function of temperature, and when evaluated in the stellar characteristic parameters, as the star radius and temperature, it satisfies the observational constraint.

An important aspect of the NSs's system, besides the high density and the low temperature, is its strong inner magnetic field, which can impact the heat capacity. For a system composed by both, electrons and quarks in the MDCDW phase, we found that the heat capacity is not exponentially damped, while the magnetic field has the following impact: its presence redefines the system density of states that now depends on  $eB$  and also produces the Landau quantization of the energy levels. We also found that the main contribution to  $C_V$  comes from the LLL when we consider the low-temperature limit, i.e.,  $k_B T \ll E_F$ . This happens because at low temperatures, the particles in the Fermi sphere don't have sufficient energy to overcome the gap between Landau energy levels, which are of order  $\sqrt{eB} > T$ . Furthermore, the magnetic field is crucial for the thermal stability of the MDCDW phase. The problem is that the new structures created by the magnetic field in the Ginzburg-Landau free energy stiffen the spectrum of the thermal fluctuations in the transverse direction, thereby avoiding the Landau-Peierls instability that affect single-modulated phases at arbitrarily low temperatures [38].

We are also reporting other results that can be important to understand the physics of the

dense phases that can play a role in the inner composition of NS. Among them, we have that observing that only the electric chemical potential affects the electron Dirac distribution, while for protons both the electric and baryonic chemical potential will play a role in the proton Dirac distribution, we found that, as a consequence of the electric neutrality condition that characterizes the stellar medium, the relation  $\mu > \mu_e > m_e$  is satisfied. This result was shown in Fig. 1, for a system made up solely by protons and electrons as charged particles. We also found that in the presence of the magnetic field - for realistic values of magnetic field and baryonic density - the heat capacity of the MDCDW phase decreases when compared with the  $B = 0$  case. Similarly, the electron contribution to the NS heat capacity is reduced when the magnetic field is present. On the other hand, if we want to observe the same density of electrons for  $B = 0$  and  $B \neq 0$ , we must have for a baryonic density of  $3n_s$  a magnetic field of  $B = \frac{2\mu^2}{3} = 10^9$  G, a value that is too high for what is expected in NSs cores [4, 5, 86].

In conclusion, we found that the contribution of quarks in the MDCDW phase to the heat capacity is one order larger than that of electrons in a magnetic field and two orders larger than the low-limit observational constraint to the heat capacity, see Section 3.4. Additionally, since two quark flavors cannot ensure charge neutrality for the MDCDW phase, then we must have electrons in the system which will also significantly contribute to the NS heat capacity [68]. Hence, we can affirm that the presence of quarks cannot be ruled out by the thermodynamic constraint under consideration, as part of the composition of NSs core.

## BIBLIOGRAPHY

- [1] M. Turatto. *Classification of Supernovae*, volume 598, pages 21–36. 2003.
- [2] Dmitrii G Yakovlev, Pawel Haensel, Gordon Baym, and Christopher Pethick. Lev Landau and the concept of neutron stars. *Physics-Uspeski*, 56(3):289–295, mar 2013.
- [3] M. C. Miller, F. K. Lamb, A. J. Dittmann, S. Bogdanov, Z. Arzoumanian, K. C. Gendreau, S. Guillot, A. K. Harding, W. C. G. Ho, J. M. Lattimer, R. M. Ludlam, S. Mahmoodifar, S. M. Morsink, P. S. Ray, T. E. Strohmayer, K. S. Wood, T. Enoto, R. Foster, T. Okajima, G. Prigozhin, and Y. Soong. 887(1):L24, dec 2019.
- [4] E. J. Ferrer and A. Hackebill. Thermodynamics of neutrons in a magnetic field and its implications for neutron stars. *Phys. Rev. C*, 99:065803, Jun 2019.
- [5] Efrain J. Ferrer and Aric Hackebill. Equation of state of a magnetized dense neutron system. *Universe*, 5(5), 2019.
- [6] Dong Lai and Stuart L. Shapiro. Cold Equation of State in a Strong Magnetic Field: Effects of Inverse beta -Decay. , 383:745, December 1991.
- [7] Efrain J. Ferrer, Vivian de la Incera, Jason P. Keith, Israel Portillo, and Paul L. Springsteen. Equation of state of a dense and magnetized fermion system. *Phys. Rev. C*, 82:065802, Dec 2010.
- [8] Gordon Baym et al. From hadrons to quarks in neutron stars: a review. *Reports on Progress in Physics*, 81(5), 2018.
- [9] R. A. Broglia, F. De Blasio, G. Lazzari, M. Lazzari, and P. M. Pizzochero. Specific heat of superfluid matter in the inner crust of neutron stars. *Phys. Rev. D*, 50:4781–4785, Oct 1994.
- [10] Ka Wai Lo. Neutron star and superfluidity. Dec 2010.
- [11] E. Østgaard. Internal structure of neutron stars. In S. Hledík and Z. Stuchlík, editors, *RAGtime 2/3: Workshops on Black Holes and Neutron Stars*, pages 73–102, December 2001.
- [12] D. G. Yakovlev, O. Y. Gnedin, A. D. Kaminker, and A. Y. Potekhin. Theory of cooling neutron stars versus observations. *AIP Conference Proceedings*, 983(1):379–387, 2008.
- [13] Isaac Vidaña. Hyperons: the strange ingredients of the nuclear equation of state. *Proceedings of the Royal Society A: Mathematical, Physical and Engineering Sciences*, 474(2217):20180145, 2018.

- [14] F. Weber. Strange quark matter and compact stars. *Progress in Particle and Nuclear Physics*, 54(1):193 – 288, 2005.
- [15] A. R. Bodmer. Collapsed nuclei. *Phys. Rev. D*, 4:1601–1606, Sep 1971.
- [16] Hidezumi Terazawa, Keiichi Akama, and Yūichi Chikashige. How to Liberate Quarks from Chromodynamical Confinement. *Progress of Theoretical Physics*, 60(5):1521–1525, 11 1978.
- [17] Edward Witten. Cosmic separation of phases. *Phys. Rev. D*, 30:272–285, Jul 1984.
- [18] Eirik Samuel Berge. The structure of quark stars. Master’s thesis, 2013.
- [19] Charles Alcock, Edward Farhi, and Angela Olinto. Strange Stars. , 310:261, November 1986.
- [20] Ian Harry and Tanja Hinderer. Observing and measuring the neutron-star equation-of-state in spinning binary neutron star systems. *Classical and Quantum Gravity*, 35(14):145010, jun 2018.
- [21] D. G. Yakovlev, O. Y. Gnedin, A. D. Kaminker, and A. Y. Potekhin. Theory of cooling neutron stars versus observations. *AIP Conference Proceedings*, 983(1):379–387, 2008.
- [22] Sachiko Tsuruta. *Thermal Evolution of Neutron Stars-Current Status*.
- [23] Mark Alford, Krishna Rajagopal, and Frank Wilczek. Color-flavor locking and chiral symmetry breaking in high density qcd. *Nuclear Physics B*, 537(1):443–458, 1999.
- [24] R. Casalbuoni, R. Gatto, M. Mannarelli, G. Nardulli, and M. Ruggieri. Meissner masses in the gcfl phase of qcd. *Physics Letters B*, 605(3):362–368, 2005.
- [25] Kenji Fukushima. Analytical and numerical evaluation of the debye and meissner masses in dense neutral three-flavor quark matter. *Phys. Rev. D*, 72:074002, Oct 2005.
- [26] Sanjay Reddy and Gautam Rupak. Phase structure of two-flavor quark matter: Heterogeneous superconductors. *Phys. Rev. C*, 71:025201, Feb 2005.
- [27] Kenji Fukushima. Characterizing the larkin-ovchinnikov-fulde-ferrel phase induced by the chromomagnetic instability. *Phys. Rev. D*, 73:094016, May 2006.
- [28] Michio Hashimoto. Manifestation of instabilities in nambu–jona-lasinio type models. *Physics Letters B*, 642(1):93–99, 2006.
- [29] Mei Huang. Spontaneous current generation in the 2sc phase. *Phys. Rev. D*, 73:045007, Feb 2006.
- [30] D. V. DERYAGIN, D. YU. GRIGORIEV, and V. A. RUBAKOV. Standing wave ground state in high density, zero temperature qcd at large  $n_c$ . *International Journal of Modern Physics A*, 07(04):659–681, 1992.

- [31] E. Shuster and D.T. Son. On finite-density qcd at large  $nc$ . *Nuclear Physics B*, 573(1):434–446, 2000.
- [32] E.J. Ferrer and V. de la Incera. Novel topological effects in dense qcd in a magnetic field. *Nuclear Physics B*, 931:192–215, 2018.
- [33] Bo Feng, Efrain J. Ferrer, and Israel Portillo. Lack of debye and meissner screening in strongly magnetized quark matter at intermediate densities. *Phys. Rev. D*, 101:056012, Mar 2020.
- [34] Herbert B Callen. *Thermodynamics and an introduction to thermostatistics; 2nd ed.* Wiley, New York, NY, 1985.
- [35] Silvio Roberto Azevedo Salinas. *Introdução à Física Estatística.* EdUSP, 1997.
- [36] N. K. Glendenning. *Compact Stars. Nuclear Physics, Particle Physics and General Relativity.* Springer, New York, 2000.
- [37] Efrain J. Ferrer and Vivian de la Incera. Magnetism in dense quark matter. *Lecture Notes in Physics*, page 399–432, 2013.
- [38] E. J. Ferrer and V. de la Incera. Absence of landau-peierls instability in the magnetic dual chiral density wave phase of dense qcd. *Phys. Rev. D*, 102:014010, Jul 2020.
- [39] R. Jackiw. Functional evaluation of the effective potential. *Phys. Rev. D*, 9:1686–1701, Mar 1974.
- [40] L. Dolan and R. Jackiw. Symmetry behavior at finite temperature. *Phys. Rev. D*, 9:3320–3341, Jun 1974.
- [41] Efrain Ferrer and Vivian Incera. Anomalous electromagnetic transport in compact stars. *Universe*, 4:54, 03 2018.
- [42] L. D. Landau. The theory of superfluidity of helium II. *J. Phys. (USSR)*, 5:71–100, 1941.
- [43] L. D. Landau. On the theory of superfluidity of helium II. *J. Phys. (USSR)*, 11:91, 1947.
- [44] Deborah N. Aguilera, Vincenzo Cirigliano, José A. Pons, Sanjay Reddy, and Rishi Sharma. Superfluid heat conduction and the cooling of magnetized neutron stars. *Phys. Rev. Lett.*, 102:091101, Mar 2009.
- [45] Paulo F. Bedaque, Gautam Rupak, and Martin J. Savage. Goldstone bosons in the  $^3P_2$  superfluid phase of neutron matter and neutrino emission. *Phys. Rev. C*, 68:065802, Dec 2003.
- [46] Paulo F. Bedaque and Sanjay Reddy. Goldstone modes in the neutron star core. *Physics Letters B*, 735:340–343, 2014.
- [47] Mark Alford, Krishna Rajagopal, and Frank Wilczek. Qcd at finite baryon density: nucleon droplets and color superconductivity. *Physics Letters B*, 422(1):247–256, 1998.

- [48] Mark Alford, Chris Kouvaris, and Krishna Rajagopal. Evaluating the gapless color-flavor locked phase. *Phys. Rev. D*, 71:054009, Mar 2005.
- [49] Efrain Ferrer. Magnetism in cold-dense qcd. page 006, 03 2012.
- [50] Efrain J. Ferrer, Vivian de la Incera, and Cristina Manuel. Magnetic color-flavor locking phase in high-density qcd. *Phys. Rev. Lett.*, 95:152002, Oct 2005.
- [51] Efrain J. Ferrer, Vivian de la Incera, and Cristina Manuel. Color-superconducting gap in the presence of a magnetic field. *Nuclear Physics B*, 747(1):88–112, 2006.
- [52] Efrain J Ferrer, Vivian de la Incera, and Cristina Manuel. Colour superconductivity in a strong magnetic field. *Journal of Physics A: Mathematical and General*, 39(21):6349–6355, may 2006.
- [53] R Casalbuoni and R Gatto. Effective theory for color-flavor locking in high density qcd. *Physics Letters B*, 464(1):111–116, 1999.
- [54] D. T. Son and M. A. Stephanov. Inverse meson mass ordering in the color-flavor-locking phase of high-density qcd. *Phys. Rev. D*, 61:074012, Feb 2000.
- [55] D. T. Son and M. A. Stephanov. Erratum: Inverse meson mass ordering in the color-flavor-locking phase of high-density qcd [phys. rev. d 61, 074012 (2000)]. *Phys. Rev. D*, 62:059902, Jul 2000.
- [56] V. A. Miransky and I. A. Shovkovy. Magnetic catalysis and anisotropic confinement in qcd. *Phys. Rev. D*, 66:045006, Aug 2002.
- [57] Igor A. Shovkovy and Paul J. Ellis. Thermal conductivity of dense quark matter and cooling of stars. *Phys. Rev. C*, 66:015802, Jul 2002.
- [58] D. Bailin and A. Love. Superfluidity and superconductivity in relativistic fermion systems. *Physics Reports*, 107(6):325–385, 1984.
- [59] Mark Alford, Jürgen Berges, and Krishna Rajagopal. Magnetic fields within color superconducting neutron star cores. *Nuclear Physics B*, 571(1):269–284, 2000.
- [60] E. V. Gorbar. Color superconductivity in an external magnetic field. *Phys. Rev. D*, 62:014007, May 2000.
- [61] L. Paulucci, Efrain J. Ferrer, Vivian de la Incera, and J. E. Horvath. Equation of state for the magnetic-color-flavor-locked phase and its implications for compact star models. *Phys. Rev. D*, 83:043009, Feb 2011.
- [62] Bo Feng, Efrain J. Ferrer, and Vivian de la Incera. Cooper pairs  $\square$  magnetic moment in mcfl color superconductivity. *Nuclear Physics B*, 853(2):213–239, 2011.



- [63] Efrain J. Ferrer and Vivian de la Incera. Magnetic phases in three-flavor color superconductivity. *Phys. Rev. D*, 76:045011, Aug 2007.
- [64] Mark G. Alford, Andreas Schmitt, Krishna Rajagopal, and Thomas Schäfer. Color superconductivity in dense quark matter. *Rev. Mod. Phys.*, 80:1455–1515, Nov 2008.
- [65] Roberto Anglani, Roberto Casalbuoni, Marco Ciminale, Nicola Ippolito, Raoul Gatto, Massimo Mannarelli, and Marco Ruggieri. Crystalline color superconductors. *Rev. Mod. Phys.*, 86:509–561, Apr 2014.
- [66] I. E. Frolov, V. Ch. Zhukovsky, and K. G. Klimenko. Chiral density waves in quark matter within the nambu–jona-lasinio model in an external magnetic field. *Phys. Rev. D*, 82:076002, Oct 2010.
- [67] S. P. Klevansky. The nambu—jona-lasinio model of quantum chromodynamics. *Rev. Mod. Phys.*, 64:649–708, Jul 1992.
- [68] S. Carignano, E. J. Ferrer, V. de la Incera, and L. Paulucci. Crystalline chiral condensates as a component of compact stars. *Phys. Rev. D*, 92:105018, Nov 2015.
- [69] E.J. Ferrer and V. de la Incera. Dissipationless hall current in dense quark matter in a magnetic field. *Physics Letters B*, 769:208–212, 2017.
- [70] Toshitaka Tatsumi, Kazuya Nishiyama, and Shintaro Karasawa. Novel lifshitz point for chiral transition in the magnetic field. *Physics Letters B*, 743:66–70, 2015.
- [71] Mei Huang and Igor A. Shovkovy. Screening masses in a neutral two-flavor color superconductor. *Phys. Rev. D*, 70:094030, Nov 2004.
- [72] Ioannis Giannakis and Hai-Cang Ren. Chromomagnetic instability and the loff state in a two flavor color superconductor. *Physics Letters B*, 611(1):137–146, 2005.
- [73] A. I. Larkin and Y. N. Ovchinnikov. Nonuniform state of superconductors. *Zh. Eksp. Teor. Fiz.*, 47:1136–1146, 1964.
- [74] Peter Fulde and Richard A. Ferrell. Superconductivity in a strong spin-exchange field. *Phys. Rev.*, 135:A550–A563, Aug 1964.
- [75] Mark Alford, Jeffrey A. Bowers, and Krishna Rajagopal. Crystalline color superconductivity. *Phys. Rev. D*, 63:074016, Mar 2001.
- [76] Jeffrey A. Bowers and Krishna Rajagopal. Crystallography of color superconductivity. *Phys. Rev. D*, 66:065002, Sep 2002.
- [77] Roberto Casalbuoni and Giuseppe Nardulli. Inhomogeneous superconductivity in condensed matter and qcd. *Rev. Mod. Phys.*, 76:263–320, Feb 2004.

- [78] Efrain J. Ferrer and Vivian de la Incera. Chromomagnetic instability and induced magnetic field in neutral two-flavor color superconductivity. *Phys. Rev. D*, 76:114012, Dec 2007.
- [79] Andrew Cumming, Edward F. Brown, Farrukh J. Fattoyev, C. J. Horowitz, Dany Page, and Sanjay Reddy. Lower limit on the heat capacity of the neutron star core. *Phys. Rev. C*, 95:025806, Feb 2017.
- [80] James M. Lattimer, C. J. Pethick, Madappa Prakash, and Pawel Haensel. Direct urca process in neutron stars. *Phys. Rev. Lett.*, 66:2701–2704, May 1991.
- [81] Charles Alcock, Edward Farhi, and Angela Olinto. Strange Stars. , 310:261, November 1986.
- [82] Edward F. Brown and Andrew Cumming. MAPPING CRUSTAL HEATING WITH THE COOLING LIGHT CURVES OF QUASI-PERSISTENT TRANSIENTS. *The Astrophysical Journal*, 698(2):1020–1032, may 2009.
- [83] Dany Page and Sanjay Reddy. Forecasting neutron star temperatures: Predictability and variability. *Phys. Rev. Lett.*, 111:241102, Dec 2013.
- [84] Turlione, A., Aguilera, D. N., and Pons, J. A. Quiescent thermal emission from neutron stars in low-mass x-ray binaries. *A&A*, 577:A5, 2015.
- [85] Michael Buballa and Stefano Carignano. Inhomogeneous chiral symmetry breaking in dense neutron-star matter. *The European Physical Journal A*, 52(3), Mar 2016.
- [86] Christian Y. Cardall, Madappa Prakash, and James M. Lattimer. Effects of strong magnetic fields on neutron star structure. *The Astrophysical Journal*, 554(1):322–339, Jun 2001.

## BIOGRAPHICAL SKETCH

Pedro Paulo Barboza Sanson was born on June 1, 1998, in São Paulo, Brazil. In 2019 he received his B.Sc in Physics from Universidade Federal de Santa Catarina, where he also finished the Honours Course PAM (Advanced Program in Mathematics) in 2017. He then completed his Master of Science (MS) in Physics under the supervision of Efrain J. Ferrer in Theoretical High-energy physics and Astrophysics in 2021 at University of Texas Rio Grande Valley.

Permanent address: Av. Gaivotas, Apt 505F Atria, 520 - Lagoa dos Ingleses, Nova Lima - MG, 34018-008, Brazil

Email: [pedropaulo.barbozasanson01@utrgv.edu](mailto:pedropaulo.barbozasanson01@utrgv.edu)